Available online at www.sciencedirect.com
ScienceDirect
Estuarine, Coastal and Shelf Science 74 (2007) 175–196
ESTUARINE COASTAL AND SHELF SCIENCE
www.elsevier.com/locate/ecss

A simple model for forecast of coastal algal blooms

Ken T.M. Wong [a], Joseph H.W. Lee [a,*], I.J. Hodgkiss [b]

[a] Department of Civil Engineering, The University of Hong Kong, Pokfulam Road, Hong Kong, P.R. China
[b] Department of Ecology and Biodiversity, The University of Hong Kong, Pokfulam Road, Hong Kong, P.R. China

Received 8 November 2006; accepted 4 April 2007
Available online 5 June 2007

Abstract

In eutrophic sub-tropical coastal waters around Hong Kong and South China, algal blooms (more often called red tides) due to the rapid growth of microscopic phytoplankton are often observed. Under favourable environmental conditions, these blooms can occur and subside over rather short time scales—in the order of days to a few weeks. Very often, these blooms are observed in weakly flushed coastal waters under calm wind conditions—with or without stratification. Based on high-frequency field observations of harmful algal blooms at two coastal mariculture zones in Hong Kong, a mathematical model has been developed to forecast algal blooms. The model accounts for algal growth, decay, settling and vertical turbulent mixing, and adopts the same assumptions as the classical Riley, Stommel and Bumpus model (Riley, G.A., Stommel, H., Bumpus, D.F., 1949. Quantitative ecology of the plankton of the western North Atlantic. Bulletin of the Bingham Oceanographic Collection Yale University 12, 1–169). It is shown that for algal blooms to occur, a vertical stability criterion, $E < 4\mu l^2/\pi^2$, must be satisfied, where E, μ, l are the vertical turbulent diffusivity, algal growth rate, and euphotic layer depth respectively. In addition, a minimum nutrient threshold concentration must be reached. Moreover, with a nutrient competition consideration, the type of bloom (caused by motile or non-motile species) can be classified. The model requires as input simple and readily available field measurements of water column transparency and nutrient concentration, and representative maximum algal growth rate of the motile and non-motile species. In addition, with the use of three-dimensional hydrodynamic circulation models, simple relations are derived to estimate the vertical mixing coefficient as a function of tidal range, wind speed, and density stratification. The model gives a quick assessment of the likelihood of algal bloom occurrence, and has been validated against field observations over a 4-year period. The model helps to explain the observed spatial and temporal patterns of bloom occurrences in relation to the vertical turbulence and nutrient condition. The success of the model points the way to the development of real time management models for disaster mitigation.

Keywords: red tides; algal blooms; red tide forecasting model; hydrodynamics; ecology; water quality modelling

1. Introduction

Over the past two decades, algal blooms (or more often called red tides) have been frequently observed in Hong Kong's coastal waters (on average 20–30 per year). These algal blooms often cause discoloration of the marine water which can lead to beach closures; in some cases they also result in severe dissolved oxygen depletion, fish kills, and shellfish poisoning. In particular, in April 1998, a devastating algal bloom (due to the dinoflagellate *Karenia digitata*) resulted in the worst fish kill in Hong Kong's history (Yang and Hodgkiss, 2004). It destroyed over 80 percent (3400 tonnes) of cultured fish stock, with estimated loss of more than HK$312 million (Lee and Qu, 2004). Worldwide, harmful algal blooms (HAB) have also become more frequent, more extensive, and more severe (Hallegraeff, 1993; Anderson, 1994).

Whereas the general ecological response of phytoplankton to environmental conditions has been extensively studied, the causality and dynamics of algal blooms are not well understood, particularly in the sub-tropical coastal waters around Hong Kong (Lee et al., 2005). Most studies concentrated on the ecophysiology of the causative species, with very few attempts to

* Corresponding author.
E-mail address: hreclhw@hkucc.hku.hk (J.H.W. Lee).

0272-7714/$ - see front matter © 2007 Elsevier Ltd. All rights reserved.
doi:10.1016/j.ecss.2007.04.012

explain the causality through intensive data collection during the blooms. Theoretical development has also been hampered by the lack of continuous field observations of the changes in hydrographic and water quality parameters during the blooms. During 2000–2003, as part of a group research project, a systematic field and modelling study of algal blooms has been carried out in Hong Kong (Lee et al., 2005). A real time telemetric monitoring system has been successfully developed to provide continuous observations at two coastal mariculture zones with distinct hydrographic and pollution loading characteristics: Kat O and Lamma Island (Fig. 1). At each of the two field stations (depth around 10 m), the chlorophyll fluorescence, dissolved oxygen (DO), and water temperature are continuously monitored at three depths, along with solar radiation, wind speed and direction, and tidal current. These near-continuous measurements are supplemented by direct *in situ* measurements of water transparency (Secchi disk depth), vertical profiles of salinity and temperature, and water sampling for nutrient (phosphate, total inorganic nitrogen) concentration at intervals of 10–14 days. Details of the real time telemetric coastal observing system have been reported (Wong, 2004; Lee et al., 2005). The collective field data suggest that the different types of observed blooms (non-motile vs. motile species) are highly correlated with the hydrodynamic and algal growth characteristics. Bloom formation depends strongly on the interaction of physical and ecological factors.

The importance of vertical processes and water column stability on algal bloom formation has long been observed by many researchers (e.g. Ryther, 1955; Margalef et al., 1979; Watanabe et al., 1995). It is well known that solar radiation and inorganic nutrients are the primary energy and material sources for autotrophic phytoplankton. The successful utilisation of light and nutrient sources determines primarily the success of an algal species. In nature, solar radiation is always received from the surface while nutrients may come from material regeneration at the sea bed. Vertical processes hence play important roles in the formation of algal blooms (Cullen and MacIntyre, 1998). Furthermore, in eutrophic coastal waters, anthropogenic nutrient input (e.g. from terrestrial runoff, riverine input, organic pollution from sewage outfall and/or mariculture activities) is also believed to contribute to algal blooms (e.g. Hodgkiss and Ho, 1997). There have however been limited quantitative studies on the conditions governing algal bloom formation. Based on sparse data from ship cruises or monthly monitoring data, some studies have led to qualitative correlation of seasonal and spatial bloom patterns with tidal mixing and vertical stratification, and riverine input (e.g. Pinegree et al., 1976; Yin, 2003).

Several mathematical models have been developed to examine factors governing a stable vertical algal profile and the formation of algal blooms. A classical study (Riley et al., 1949) used the vertical mass transport equation to examine the sustainability of a quasi-steady vertical algal concentration profile in a water body of large depth. Riley et al.'s idea was further developed (Di Toro, 1974; Schnoor and Di Toro, 1980) to study the relative importance of algal settling, vertical mixing, light

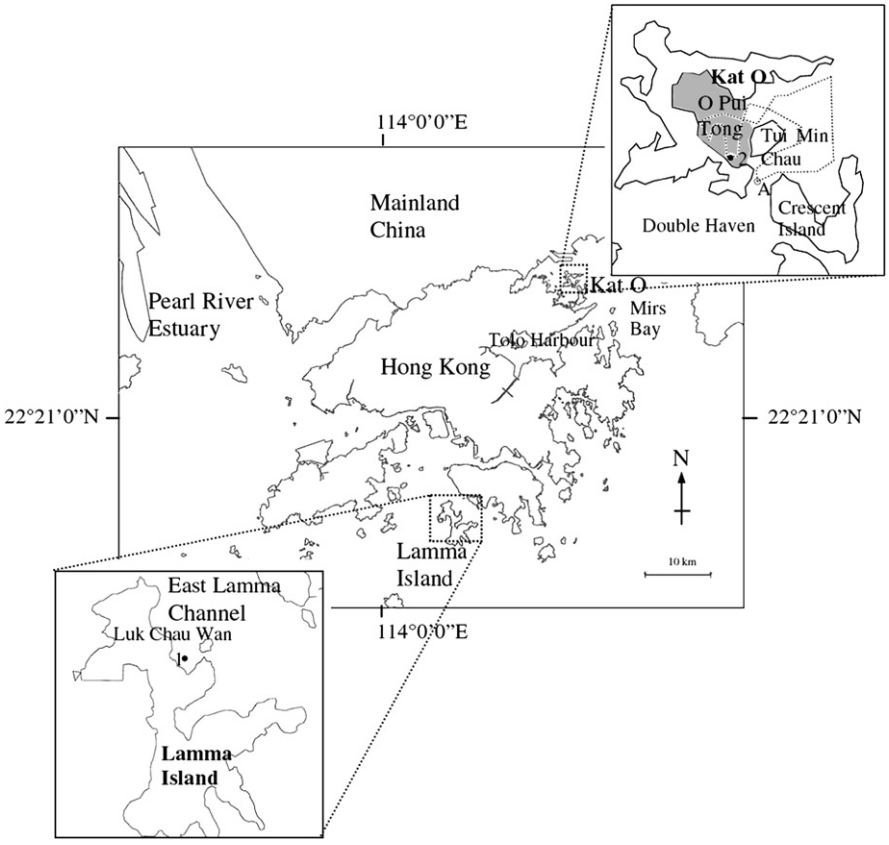

Fig. 1. Location map of Hong Kong and the two field monitoring stations (1. Lamma Island station; 2. Kat O station).

penetration and algal growth; the model was used to estimate algal settling velocities from field data of blooms over rather long time scales (typically of the order of several months). Sverdrup (1953) proposed the classic critical depth model to predict algal blooms whenever the mixing layer depth becomes shallower than the critical depth. Based on the critical depth idea, Huisman et al. (1999) used a numerical model to show the suitability of different types of habitats for algal bloom formation. However, these studies of physical-biological interaction are primarily conceptual models aimed to extract insights from long-term field observations, and the issue of short-term bloom forecasting is not addressed. A direct linkage of environmental forcing variables (e.g. tidal flow) with field data of algal blooms is lacking, and there is no clear quantitative framework to determine the model parameters or to test the models. In addition, all the previous models assume the phytoplankton are purely sinking, while in reality, most harmful algae are motile (Paerl, 1988; Smayda, 1997a).

In this article, we present a simple vertical stability theory and algal bloom prediction model framework for field application in coastal shallow water. Our objective is to derive practical metrics to interpret the complex myriad of field observations, and to develop a first order model for assessing the likelihood of bloom events. The theory is based on the approach of Riley et al. (1949) and Di Toro (1974). We further develop the idea to infer the conditions for the phytoplankton to bloom, maintain a steady state or die off under different water column stability and growth status. It is shown that certain water stability conditions are necessary for blooms of both non-motile and motile species; the threshold value of vertical diffusivity for bloom formation is derived. A simple model is then developed to predict the likelihood of algal bloom occurrences at a given location. In addition, with the use of three-dimensional hydrodynamic circulation models, we outline a robust method to predict the representative vertical mixing characteristics in semi-enclosed tidal inlets as a function of tidal range, wind, and vertical stratification. Further, the importance of vertical turbulent mixing in controlling nutrient supply to motile and non-motile species is also studied; based on the competitive advantage of securing nutrient supply, a nutrient-stability criterion is developed to distinguish between the two types of blooms. The algal bloom prediction model requires as input only generally available algal growth parameters, and minimal field measurements; it has been shown to be successful in predicting algal bloom occurrences in semi-enclosed coastal waters such as Kat O and Lamma Island.

2. Summary of field observations

The present red tide forecast model is motivated by field observations. Over the 2000–2003 period, 21 algal blooms have been monitored at these two stations. It has been observed that diatoms are always dominating at the Lamma Island station where the estuarine flow is significantly influenced by the Pearl River (Fig. 1), with typical tidal velocities of 15–20 cm s^{-1}. Blooms of diatoms often occur in the summer wet season when the water body is moderately to weakly stratified and nutrient levels are high (Lee et al., 2005). In the semi-enclosed northeastern waters around Kat O, the water body is generally much calmer (typical velocity 1–5 cm s^{-1}), and nutrient conditions are much more limiting. Blooms of dinoflagellates are more frequently observed in the Spring, under weakly- or un-stratified conditions.

The physical hydrography of Hong Kong waters is mainly influenced by three factors: tidal currents, monsoon-affected ocean currents, and the Pearl River discharges. Tides in Hong Kong are mixed and mainly semi-diurnal, with a mean tidal range of 1.7 m. In the dry season (October to March), the predominant wind direction is E/NE; and the predominant coastal current flows from NE to SW. The salinity is approximately vertically homogenous (well-mixed), and the south- to northeastern waters are unaffected by the Pearl River. In the wet season, the predominant coastal current flows from W/SW to E/NE along with the southwest monsoon wind. The interaction of the Pearl River discharge and the tidal currents create significant horizontal and vertical salinity gradients in the western and southern waters (where Lamma Island is located). However, the eastern waters are more oceanic and relatively sheltered from the Pearl River. Long-term water quality monitoring data by the Hong Kong environmental protection department also reveals a significant increase of nutrient concentration in the western waters in the wet season (due to Pearl River input), while the eastern waters are relatively unaffected (Lee et al., 2006). In particular, the nutrient level inside Mirs Bay (where Kat O is located) is not influenced by the Pearl River discharge; nutrient levels are mainly related to the water quality of the coastal current, terrestrial runoff and local pollution. A detailed account of the complex tidal flow and salinity structure of the Hong Kong waters can be found in Lee et al. (2006).

Fig. 2 shows the short-term dynamics of a bloom caused by mixed diatom species observed at Lamma Island in August 2000. It can be observed that the algae can grow to very high concentrations and also subside within a rather short period. In general, an algal bloom is accompanied by corresponding changes in nutrient concentration, water transparency, and dissolved oxygen. The low wind speed and the vertical temperature stratification preceding and during the bloom can be noted.

Broadly speaking, bloom-forming algae can be categorised into non-motile and motile species (notably diatoms and dinoflagellates in marine systems). Diatoms are suspended in the water, and rely on passive advection and diffusion to obtain their nutrient supply. The variation in vertical algal concentration is generally rather gradual during a diatom bloom (Fig. 3a). On the other hand, the dinoflagellates can migrate vertically in a diurnal pattern: swimming down towards the sea bed to fetch nutrients during the night, and up towards the surface to obtain sunlight during the day (Fig. 3b). A clear layer formation and vertical migration pattern can be observed for the species. This vertical pattern is distinctive from the much more uniform vertical algal distribution of a diatom bloom. These general features are shared by all the blooms we observed (Wong, 2004; Lee et al., 2005).

As noted by Smayda (1997a), over 90% of the harmful algal species are flagellates (notably dinoflagellates). In principle, the ecophysiological characteristics of HAB flagellates are significantly different from diatoms (the non-motile species);

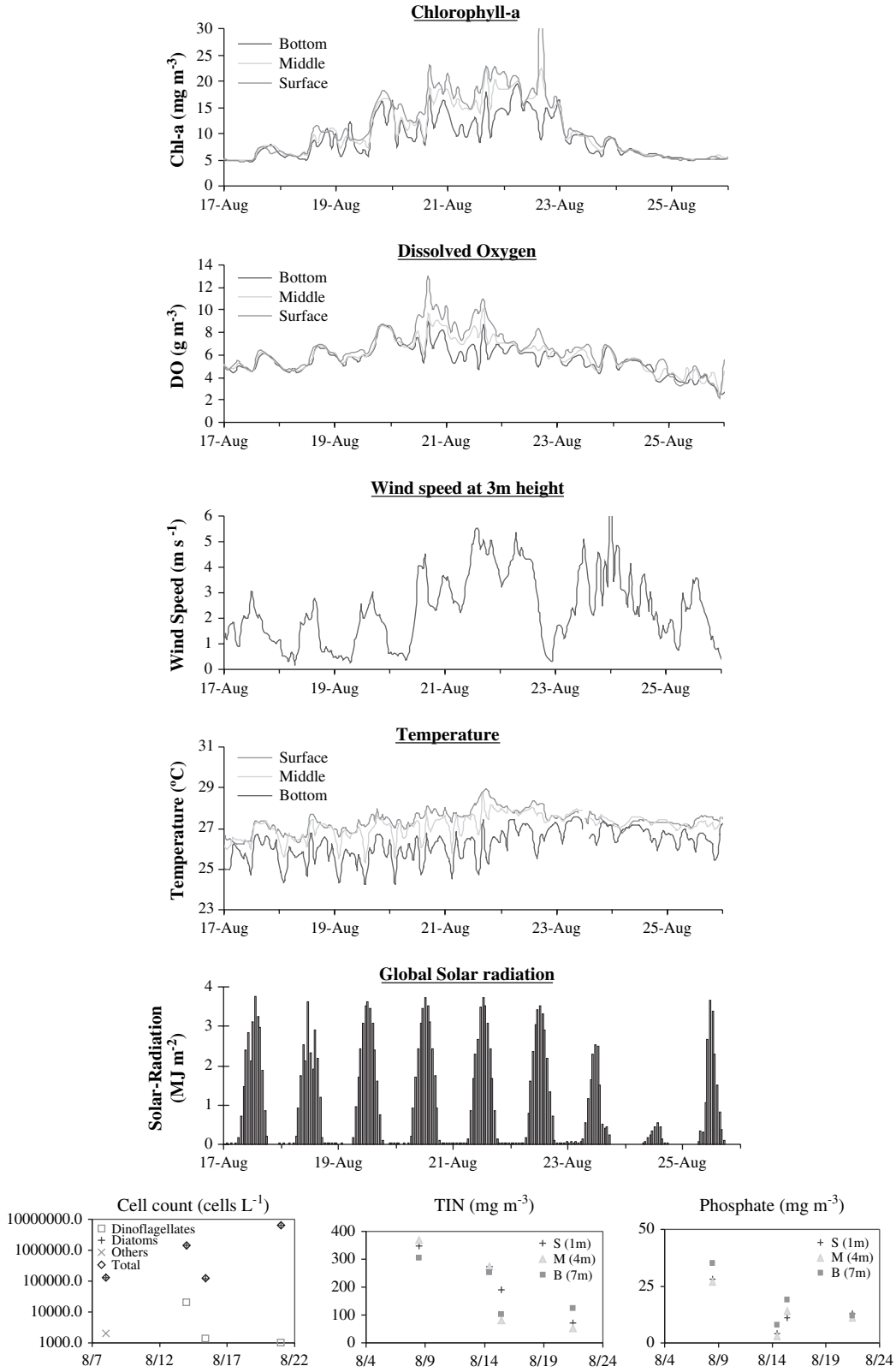

Fig. 2. Observed variations in water quality during a mixed diatom bloom (Lamma Island) in August 2000.

namely their vulnerability to turbulence, lower growth rate, different nutrient affinity, and motility. Therefore, it is not only necessary to identify the conditions favouring algal blooms but also conditions contributing to the competitive advantage of motile species against their non-motile counterpart. Margalef (1978) showed that the selection of dinoflagellates and diatoms is strongly governed by the nutrient availability and turbulence intensity. Due to their swimming behaviour, nutrient replenishment

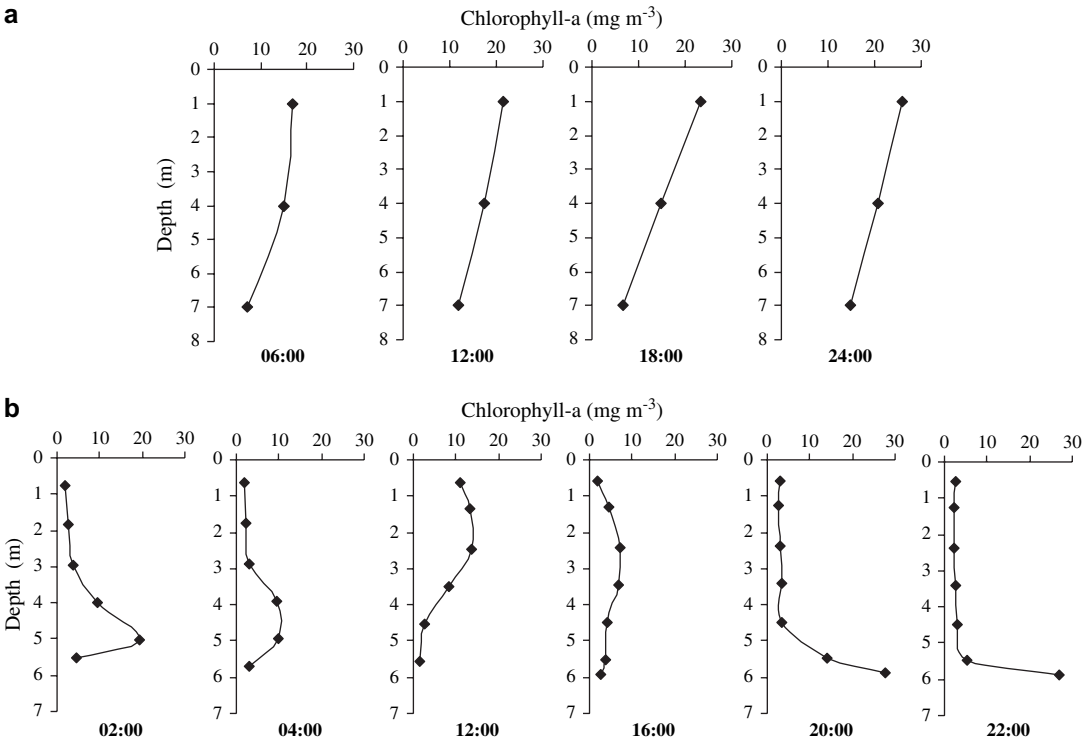

Fig. 3. Observed algal concentration profiles during blooms of (a) diatoms (August 2000, Lamma Island) and (b) dinoflagellates (March 2001, Kat O).

for dinoflagellates can be much more efficient than diatoms in nutrient-depleted stratified waters (“K-strategy”). On the other hand, in nutrient-replete turbulent waters, nutrient supply is less limiting and the fast growing diatoms will become dominating (“r-strategy”). Although the above works are useful for a qualitative understanding of the species succession sequence, they do not provide a quantitative framework for parameter identification and bloom prediction.

In the following, we develop a vertical stability criterion to establish the necessary conditions for algal blooms in a water body of finite depth, and a simple nutrient stability criterion to distinguish diatom and dinoflagellate blooms.

3. HAB forecast model

3.1. Bloom formation by non-motile species (diatoms)

We adopt the two-layer model proposed by Riley et al. (1949), in which the changes in phytoplankton biomass in a water column is assumed to depend on phytoplankton growth, loss due to mortality and predation, turbulent diffusion, and algal settling (Fig. 4). The water column is simplified as one consisting of an upper euphotic layer of thickness l and net phytoplankton growth rate μ, and a lower layer extending from l to H with mortality rate d. The time variation of algal biomass in the euphotic layer ($0 \le z \le l$) is governed by the advective diffusion equation along the water depth z:

$$\frac{\partial C}{\partial t} = E\frac{\partial^2 C}{\partial z^2} - v\frac{\partial C}{\partial z} + \mu C \tag{1}$$

where $C(z, t)$ = algal concentration, E = vertical turbulent diffusivity, and v is the sinking velocity. In this first order theory, all the parameters are assumed to be constant. A similar equation applies for the lower layer ($l \le z \le H$):

$$\frac{\partial C}{\partial t} = E\frac{\partial^2 C}{\partial z^2} - v\frac{\partial C}{\partial z} - dC \tag{2}$$

where d is the mortality and loss rate. Eqs. (1) and (2) can be solved to obtain the time-dependent vertical algal distribution, subject to the initial condition $C(z, 0)$ and prescribing the boundary conditions of: (a) zero mass flux condition at the surface ($z = 0$),

$$vC - E\frac{\partial C}{\partial z} = 0;$$

(b) continuity of concentration and mass flux at the interface, $z = l$; and (c) a boundary condition at the sea bed, $z = H$.

3.1.1. Solution for infinite depth

For the case of large depth ($H \to \infty$), the condition at the lower boundary is $C \to 0, z \to \infty$. Di Toro (1974) has shown that an asymptotic solution of the form $C = f(z)e^{kt}$ exists, where k is the population net growth rate accounting for the effect of growth, mortality, and mass transport, and $f(z)$ is given by:

$$f(z) = Ke^{(az)}(\beta\cos\ \beta z + a\sin\ \beta z) \quad \text{for } z \le l \tag{3}$$

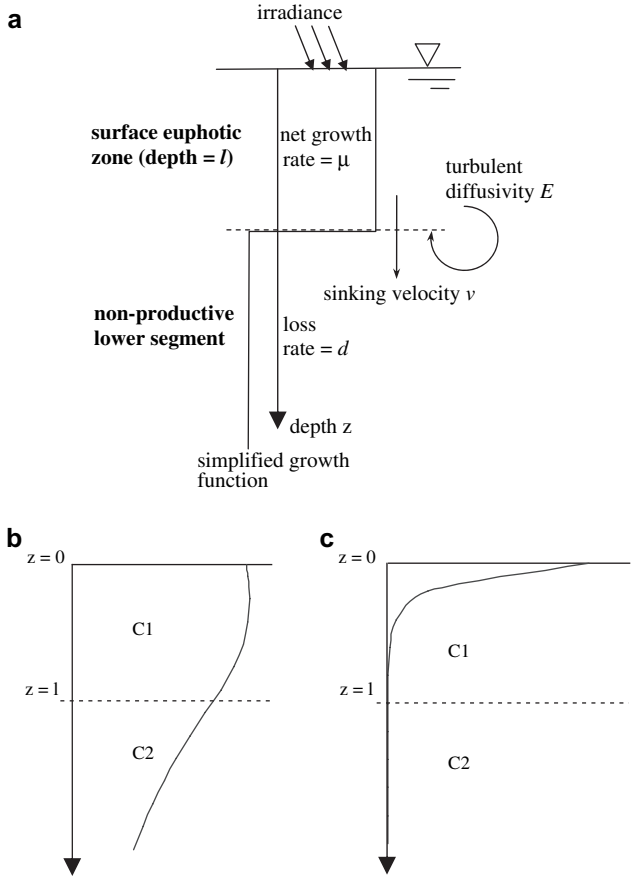

Fig. 4. (a) Simplified algal dynamics model for a water column. (b) Concentration profile for non-motile species. (c) Concentration profile for motile species (upward migration only).

$$f(z) = Ke^{(az)}e^{-b(z-l)}(\beta\cos\ \beta l + a\sin\ \beta l) \quad \text{for } z \geq l \tag{4}$$

where $a = v/2E$, $b = \sqrt{v^2/4E^2 + (d+k)/E}$, $\beta = \sqrt{(\mu-k)/E - v^2/4E^2}$, and K is a constant that depends on the initial condition. In addition, for the solution to exist, the model parameters must satisfy the following condition (an eigen-condition):

$$\tan\ \beta l = \frac{\beta(a+b)}{(\beta^2 - ab)} \tag{5}$$

For given values of μ, E, l, v, d, Eq. (5) can be solved to obtain the net growth rate k (the eigen-value). For positive k, biomass in the water column will increase monotonically and an algal bloom will be implied. For negative k, the biomass will collapse and a bloom cannot be formed. For $k = 0$, the quasi-steady condition, Eq. (5) reduces to the existence condition for a steady profile derived by Riley et al. (1949) who obtained the same form of the spatial distribution $f(z)$. In particular, Riley et al. (1949) has shown that if $\mu < v^2/4E$, the algal population will always decrease due to sinking loss, and a steady state profile is not possible.

It should be noted that a numerical solution of the time evolution of the algal distribution $C(z, t)$ is needed for a comprehensive study of algal bloom stability and the determination of the coefficient K in the spatial distribution. This however was not addressed by the above works of Riley et al. and Di Toro.

3.1.2. Solution for finite depth

For the case of finite depth, following the same analytical approach, and after imposition of (a) zero mass flux boundary condition at the free surface, $z = 0$, (b) continuity of concentration and mass flux at the interface, $z = l$, the asymptotic solution for the upper and lower layers can be shown to be $C(z, t) = f(z)e^{kt}$, where

$$f(z) = Ke^{az}(\beta\cos\ \beta z + a\sin\ \beta z) \quad \text{for } z \leq l \tag{6}$$

$$f(z) = \frac{Ke^{az}}{2b}\Big(\big[(a+b)\beta\cos\ \beta l + (ab-\beta^2)\sin\ \beta l\big]e^{b(z-l)} + \big[(b-a)\beta\cos\ \beta l + (ab+\beta^2)\sin\ \beta l\big]e^{-b(z-l)}\Big) \quad \text{for } l \leq z \leq H \tag{7}$$

It can be seen the upper layer concentration is the same as that obtained for infinite depth. To investigate the algal bloom condition, consider the most conservative case with $C = 0$ at the sea bed ($z = H$). For this case, putting $f(z) = 0$ at $z = H$, the solution must satisfy the following eigen-condition:

$$\big[(a+b)\beta\cos\ \beta l + (ab-\beta^2)\sin\ \beta l\big]e^{b(H-l)} + \big[(b-a)\beta\cos\ \beta l + (ab+\beta^2)\sin\ \beta l\big]e^{-b(H-l)} = 0$$

$$\tan\ \beta l = \frac{\beta(a+b) + \beta(b-a)e^{-2b(H-l)}}{(\beta^2 - ab) - (\beta^2 + ab)e^{-2b(H-l)}} \tag{8}$$

From Eq. (8), it can be observed that as $H \to \infty$, the eigen-condition for infinite depth (Eq. 5) is recovered. Further, when the euphotic zone depth is equal to the total depth, $l = H$, Eq. (8) becomes

$$\tan\ \beta l = \frac{-\beta}{a} \tag{9}$$

3.2. Algal bloom stability

The possibility of algal blooms is best illustrated by a numerical solution of the full unsteady mass conservation equation for the algal biomass (Eqs. 1 and 2) for a water column of finite depth. Given the values of net algal growth rate and euphotic depth (μ and l), mortality rate in lower layer d, algal settling velocity v, turbulent diffusivity E and water depth H, the time variation of algal biomass $C(z, t)$ can be obtained by a finite difference solution of the governing equation. Starting from an assumed initial condition, an accurate numerical solution can be readily obtained by using an explicit forward time centred space (FTCS) scheme (Roache, 1998). The time derivative $\partial C/\partial t$ is discretised with a forward difference, while the diffusion term is approximated by a second-order central difference. A zero mass flux boundary condition is imposed at the free surface ($z = 0$), and a zero concentration condition at the bottom boundary ($z = H$). Extensive numerical experimentation with different initial conditions and a wide

range of model parameters typical of Hong Kong coastal waters (water depth $H = 10–20$ m; $l = 2–8$ m; $\mu = 0.5–2$ day^{-1}; $d = 0.1–100$ day^{-1}; $v = 0.5–5$ m day^{-1}; $E = 0.0002–0.001$ m^2 s^{-1}) has been performed; a time step of $\Delta t = 60$ s and grid size $\Delta z = 1$ m are used.

The numerical results show that bloom stability is governed by two key parameters: a dimensionless growth number $G = \mu l^2/E$, and a euphotic layer Peclet number $Pe = vl/E$. Fig. 5 illustrates algal growth possibilities for three representative cases, with $H = 10$ m and $l = 5$ m. In the model run, an initial uniform algal concentration of $C(z, 0) = 5$ mg m^{-3} is imposed and the model is run for 10 days. For each case, the time evolution of the vertical algal distribution (left), and the average algal concentration in the euphotic layer (right) are shown. The net algal growth rate k can hence be determined. Several interesting observations can be made:

- Case (1) satisfies the condition $\mu < v^2/4E$ (or $G < Pe^2/4$), with $E = 0.0005$ m^2/s, $\mu = 0.01$day^{-1}, $v = 2$ m day^{-1}, and $d = 0$ day^{-1} ($G = 0.006$, $Pe^2/4 = 0.013$). It is clear a vertical structure cannot be sustained. This correlates with the collapse of an algal community. During the end of the bloom, the growth rate is very small (e.g. due to nutrient depletion or light limitation). When μ becomes less then $v^2/4E$, the bloom becomes unsustainable.
- Case (2) is growth dominated, with $E = 0.0002$ m^2/s, $\mu = 2$ day^{-1}, $v = 0.5$ m day^{-1}, and $d = 2$ day^{-1} ($G = 2.894$, $Pe^2/4 = 0.005$), the biomass production exceeds losses,

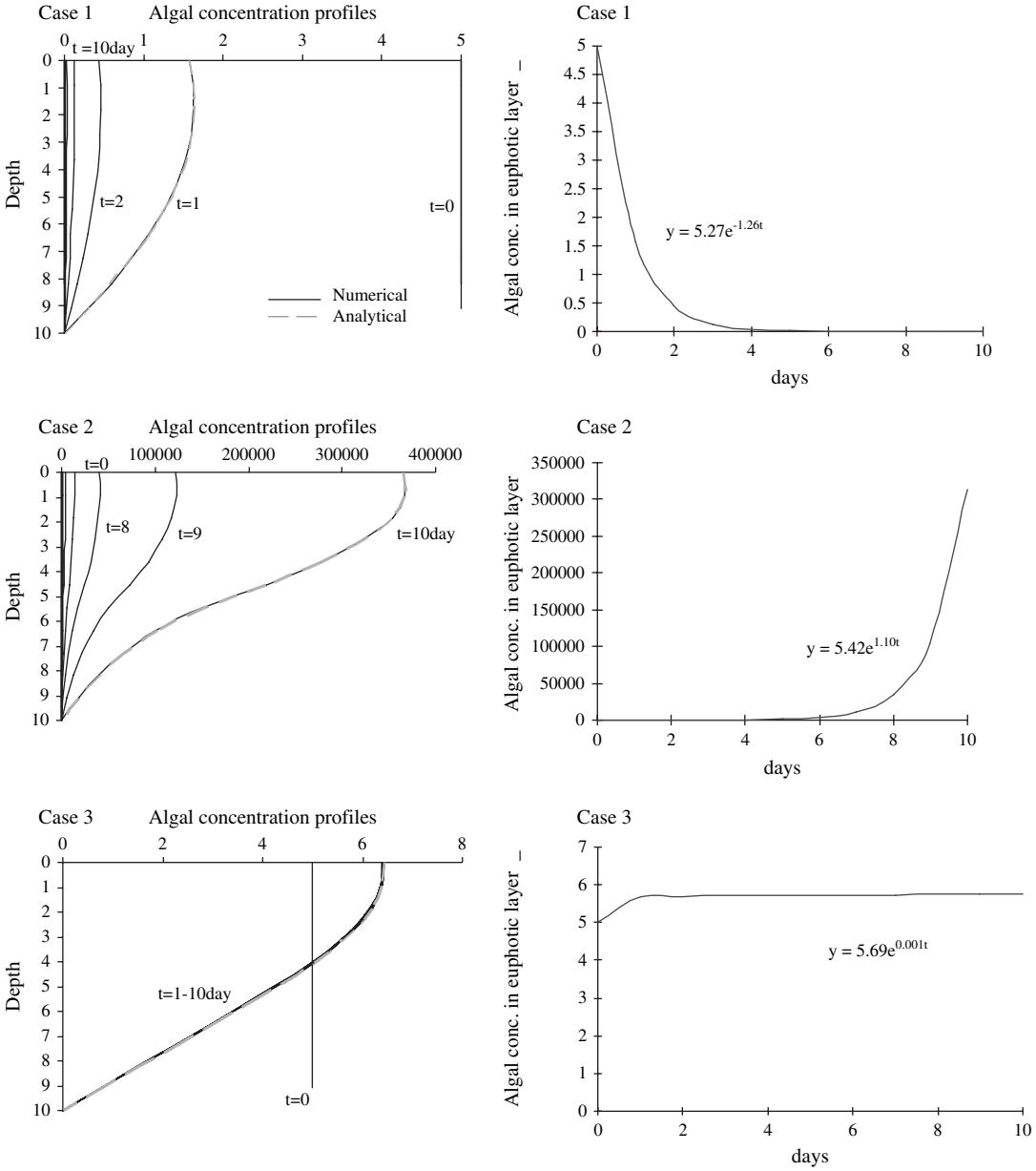

Fig. 5. Numerical solution of vertical algal concentration profile (mg m^{-3}) for three conditions. Case 1, collapse; Case 2, bloom; Case 3, quasi-steady state.

and a bloom ($k > 0$) occurs. This should correspond to the initial phase of a bloom event.

- Case (3) corresponds to a quasi-steady condition ($k = 0$), with $E = 0.000745$ m^2/s, $\mu = 2$ day^{-1}, $v = 0.5$ m day^{-1}, and $d = 0.2$ day^{-1} ($G = 1.157$, $Pe^2/4 = 0.001$). The solution converges to the steady-state quickly from the initial condition.

Other results (not shown) also reveal that: (a) the numerically determined population net growth rates are in excellent agreement with that determined from the analytical eigen-condition (e.g. for case (1), $k = -1.26$ versus the solution of Eq. 8, $k = -1.27$); (b) the computed spatial distribution converges rapidly to the form given by the analytical solution (Eqs. 6 and 7) within 1–2 days, from which the coefficient K can be determined; (c) the solution checks with Riley et al.'s solution for infinite depth. Fig. 4b) shows the solution for a typical diatom profile ($\mu = 1.5$ day^{-1}, $l = 6$ m, $v = 1$ m day^{-1}, $E = 3.5 \times 10^{-4}$ m^2 s^{-1}).

The bloom stability criterion can hence be determined numerically on a (G, Pe) diagram; this is illustrated in Fig. 6 for $l/H = 0.5$, and for $d/\mu = 0.1$ to 1. The circles and crosses are numerical runs with $k > 0$ and $k < 0$ respectively for $d = 0.1\mu$. It is seen that the stability condition conforms with the analytical eigen-condition, and is not very sensitive to the mortality rate for $d/\mu = 0.1$–1 (which should cover most cases of interest); the results are mainly dependent on the dimensionless euphotic zone depth l/H. The likelihood of algal blooms formed by non-motile species in a water column can be predicted by the stability diagram shown in Fig. 7. The stability criterion for the infinite depth case $l/H \to 0$ and Riley et al.'s collapse condition $G < Pe^2/4$ can be seen. As l/H increases, the stability bound is shifted upwards. If the upper envelope ($l/H = 1$) of the family of eigen-conditions is adopted as a conservative estimate of the likelihood of algal blooms, the stability criterion will be given by Eq. (9), with

$$\cot \beta l = \frac{-a}{\beta} = \frac{-v}{2E\beta} \tag{10}$$

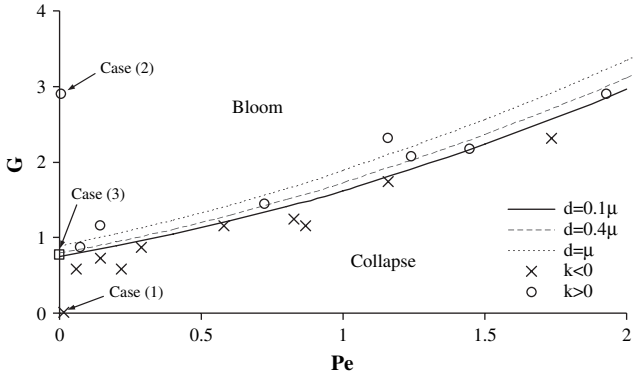

Fig. 6. Numerical stability criterion for $l/H = 0.5$ ($d = 0.1\mu$). Numerical runs (circles $k > 0$, crosses $k < 0$) are shown along with solution of the analytical stability criterion (Eq. 8) for $d/\mu = 0.1$, 0.4 and 1.

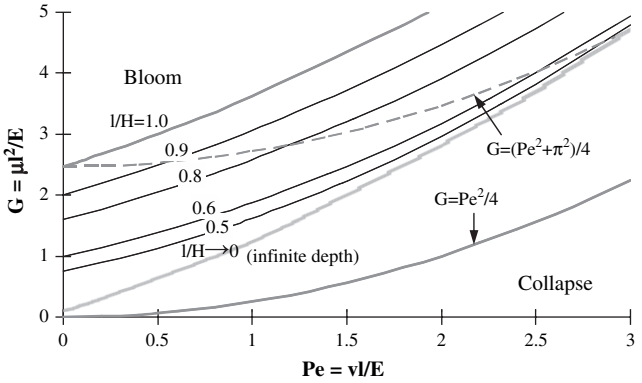

Fig. 7. Stability criterion for non-motile species.

From our field observations, a is always much less than β during algal blooms (see Table 3). We then have cot $\beta l \approx 0$, and

$$\beta l = l\sqrt{(\mu - k)/E - v^2/4E^2} = \pi/2$$

Therefore, k is always positive if

$$k = \mu - v^2/4E - \pi^2 E/4l^2 > 0$$

Rearranging, the bloom stability criterion can be obtained as

$$\mu l^2/E - v^2 l^2/4E^2 > \pi^2/4 \tag{11}$$

or $G = (Pe^2 + \pi^2)/4$. If Eq. (11) is fulfilled, the phytoplankton production within the euphotic layer will exceed the rate at which it diffuses and settles out of it. Therefore, an algal bloom will be predicted. It is useful to cast the bloom stability in terms of a critical turbulence criterion (Huisman et al., 1999). To obtain the range of diffusivity for which blooms would occur, Eq. (11) can be re-arranged such that E becomes the variable,

$$\pi^2 E^2 - 4\mu l^2 E + v^2 l^2 < 0 \tag{12}$$

Solving Eq. (12), we have

$$\frac{1}{\pi^2}\left(2\mu l^2 - l\sqrt{4\mu^2 l^2 - \pi^2 v^2}\right) < E < \frac{1}{\pi^2}\left(2\mu l^2 + l\sqrt{4\mu^2 l^2 - \pi^2 v^2}\right) \tag{13}$$

For most situations, $4\mu^2 l^2$ is an order greater than $\pi^2 v^2$ (see also values in Table 3). The above stability criterion then reduces to a simple expression for the allowable range of E:

$$\frac{v^2}{4\mu} < E < \frac{4\mu l^2}{\pi^2} \tag{14}$$

The lower bound for E corresponds to Riley et al.'s bloom collapse condition; the upper bound gives the threshold value for the vertical diffusivity below which an algal bloom can occur:

$$E < \frac{4\mu l^2}{\pi^2} \tag{15}$$

It is interesting to note that the sinking velocity does not enter into the approximate estimate of the critical turbulence; a good estimate on the required E can be obtained by omitting the sinking term. For example, for typical values of $\mu = 1.5\ \text{day}^{-1}$, $l = 6$ m, $v = 1\ \text{m day}^{-1}$, the threshold diffusivities estimated using Eqs. (10), (13) and (15) are $E = 2.24 \times 10^{-4}$, $E = 2.51 \times 10^{-4}$ and $E = 2.53 \times 10^{-4}\ \text{m}^2\ \text{s}^{-1}$ respectively. Note that the foregoing theoretical development tacitly assumes nutrient unlimiting conditions (see later discussion).

3.3. Bloom formation by motile species (dinoflagellates)

At day time, the motile species swim up to the water surface to harvest light. Bloom formation is hence expected to similarly depend on the vertical diffusivity, euphotic depth, algal growth rate and upward swimming speed. The stability criteria for motile species can be obtained by again considering the transport equations (1 and 2), and replacing v by $-v$ in the governing equation

$$\frac{\partial C}{\partial t} = E\frac{\partial^2 C}{\partial z^2} + v\frac{\partial C}{\partial z} + \mu C \quad \text{for } z \le l \tag{16}$$

$$\frac{\partial C}{\partial t} = E\frac{\partial^2 C}{\partial z^2} + v\frac{\partial C}{\partial z} - dC \quad \text{for } z \ge l \tag{17}$$

By assuming an asymptotic solution of the form $C(z, t) = f(z)e^{kt}$, and noting that $v^2/4E > \mu$ for typical dinoflagellates (see later discussion), it can be shown that:

$$f(z) = Ke^{-az}\left[(b'-a)e^{b'z} + (b'+a)e^{-b'z}\right] \quad \text{for } z \le l \tag{18}$$

$$f(z) = Ke^{-az}e^{-b(z-l)}\left[(b'-a)e^{b'l} + (b'+a)e^{-b'l}\right] \quad \text{for } z \ge l \tag{19}$$

where $a = v/2E$, $b' = \sqrt{v^2/4E^2 - (\mu - k)/E}$, $b = \sqrt{v^2/4E^2 + (d+k)/E}$, k is the population net growth rate and K is an arbitrary positive constant.

Similar to the case of non-motile species, a stability criteria can be obtained by considering the most conservative case with $l = H$; imposing the bottom boundary condition $C = 0$ at $z = H$ then gives

$$a + b' = (a - b')e^{2b'l} \tag{20}$$

For given values of μ, E, l, v, d, Eq. (20) can be solved to obtain b' and hence the net algal growth rate k (eigenvalue). Rewriting in terms of $Pe = vl/E = 2al$, and $x = b'l$, Eq. (20) can be recast as:

$$\frac{Pe}{2}\tanh(x) = x \tag{21}$$

Since $\tanh(x) \approx x$ for $x \ll 1$, it is clear that Eq. (21) has no solution for $Pe < 2$. From Eqs. (20) or (21) a stability diagram for bloom formation by motile species can be constructed (Fig. 8). Under steady state, $k = 0$, and Eq. (20) can be written in terms of the dimensionless growth number $G = \mu l^2/E$ and Peclet number $Pe = vl/E$ as:

$$Pe/2 + \sqrt{Pe^2/4 - G} = \left(Pe/2 - \sqrt{Pe^2/4 - G}\right)e^{2\sqrt{Pe^2/4 - G}} \tag{22}$$

Eq. (22) is shown as the stability criterion in Fig. 8. Using typical algal growth parameters (μ, l, and upward swimming speed v for dinoflagellates), a bloom can occur ($k > 0$, right hand side of Fig. 8) by decreasing E (i.e. increasing both G and Pe on the dimensionless plot). This is shown as a series of dotted lines in Fig. 8. For Peclet numbers below 2, dinoflagellate blooms will not occur. The analytical bloom stability criterion, Eq. (22), has been validated by extensive numerical tests performed with various representative parameters (water depth $h = 10$–20 m; $l = 2$–8 m; $d = 0.05$–$0.2\ \text{day}^{-1}$; $v = 0.5$–$1\ \text{m h}^{-1}$ (upward); $E = 0.00005$–$0.001\ \text{m}^2\ \text{s}^{-1}$). Fig. 4c) shows the solution for a typical dinoflagellate profile ($\mu = 0.5\ \text{day}^{-1}$, $l = 6$ m, $v = 1.0\ \text{m h}^{-1}$, $E = 2.1 \times 10^{-4}\ \text{m}^2\ \text{s}^{-1}$); surface aggregation of the upward-mobile dinoflagellates can be noted. For this high Peclet number situation ($Pe = 8$), turbulent mixing has little effect in retarding the vertical migration and surface aggregation.

If the two stability diagrams for motile and non-motile species are combined schematically (direct overlapping of the two diagrams, however, is avoided since v and μ values for the two are different), an interesting pattern can be observed (Fig. 9). For non-motile species, it is seen that bloom formation can be accomplished by increasing G (growth strategy). For motile species, a migratory strategy in which bloom formation is accomplished by increasing Pe is predicted. It is noteworthy that the above theoretical prediction is consistent with the general observations and bloom formation strategies pointed out by various authors (e.g. Cullen and MacIntyre, 1998; Smayda, 2002). As shown in the figure, there is a common region where algal blooms can be formed by both motile and

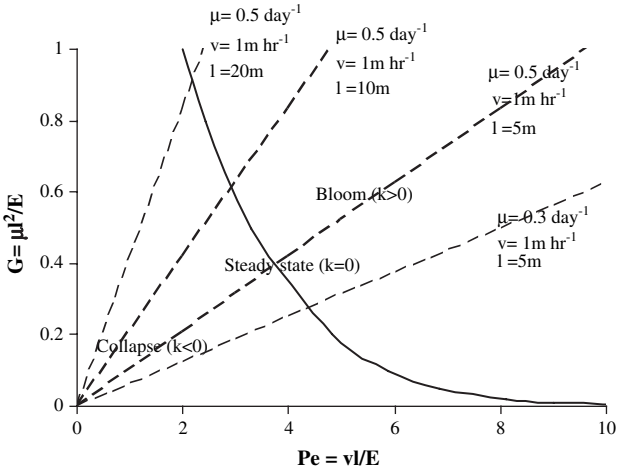

Fig. 8. Stability criterion for motile species (Eq. 22).

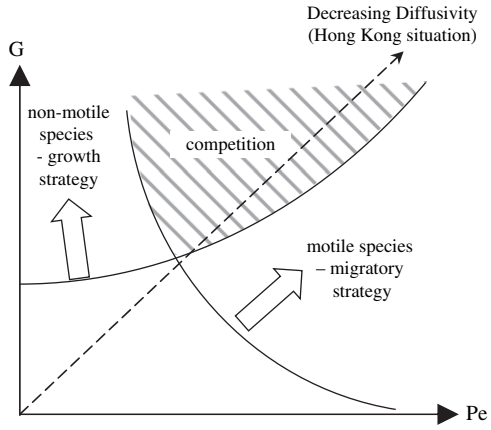

Fig. 9. Bloom formation strategy for motile and non-motile species.

non-motile species. To determine which type of bloom will actually occur, further considerations of species competition are required (see next section).

The two stability criteria for motile and non-motile species can be interpreted in terms of the required critical turbulence for bloom formation under nutrient non-limiting conditions. Using typical values of euphotic depth $l = 10$ m, dinoflagellate migration speed of 1 m h^{-1}, diatom growth rate of 1.5 day^{-1} and dinoflagellate growth rate of 0.5 day^{-1} for Hong Kong coastal waters, the required critical turbulent diffusivity values are surprisingly not very different—$E = 7.0 \times 10^{-4}$ m^2 s^{-1} for diatoms (Eq. 15) and $E = 9.27 \times 10^{-4}$ m^2 s^{-1} (Eq. 22) for dinoflagellates. Despite the similar threshold diffusivities based purely on stability considerations, our field observations show that dinoflagellates are out-competed by diatoms except in very tranquil waters. Therefore, in our application, only Eq. (15) would be used to provide a first order estimate of the likelihood of algal blooms.

3.4. Competition between motile and non-motile species

It is commonly believed that the requirement of a more tranquil environment for dinoflagellate growth may be related to cell rupturing and disorientation on migration in turbulent waters (White, 1976; Estrada et al., 1987; Thomas and Gibson, 1990). However, a recent review of experimental data on effects of turbulence on plankton shows that dinoflagellate growth will not be significantly impaired unless the turbulence energy dissipation rate reaches the order of 10^{-3} m^2 s^{-3} (Peters and Marrase, 2000). In coastal waters of typical depths and mixing lengths of the order of 10 m and 1 m respectively, this condition would correspond to vertical diffusivity of around 0.1 m^2 s^{-1}. This threshold required for physiological impediment under turbulence is much larger than the vertical diffusivity computed from the stability criterion (of the order of 10^{-4} m^2 s^{-1}). This seems to suggest that cell rupture and growth inhibition may not be the key factors for the preference for a tranquil environment in coastal waters. On the other hand, as described by Margalef's "Mandala" (Margalef, 1978) and Reynolds "Intaglio" (Reynolds, 1987), turbulence and nutrient accessibility can play a central role in species selection. Due to the fact that non-motile species (diatoms) are much faster growing, they are always the dominating species in turbulent waters where nutrients are more accessible. In tranquil waters, the nutrient accessibility is reduced due to the reduced turbulent transport. However, through vertical migration, motile species can maintain access to the sea bottom nutrient pool and have a competition advantage.

Building on the two-layer model, a comparison in the efficiencies of motile and non-motile species in harvesting bottom nutrient in tranquil waters can be made as follows (Fig. 10). Assume nutrient supply is solely from that regenerated from below the euphotic layer. For motile species, the organisms themselves act as nutrient pumps (Margalef et al., 1979). As long as the bottom nutrient pool is within reach of their migratory distance, nutrient transported up through active migratory behaviour is simply given by the amount taken up by the algal cells. If the algal concentration is presented in terms of cellular nutrient content, the nutrient uptake per unit algae per unit time will be equal to its growth rate, μ'.

For non-motile species, the supply of nutrient has to rely on the passive turbulent diffusive transport. The vertical mass balance for nutrient and algae can be written as:

$$E\frac{\partial^2 N}{\partial z^2} - \mu C = \frac{\partial N}{\partial t}$$
$$E\frac{\partial^2 C}{\partial z^2} - vC + \mu C = \frac{\partial C}{\partial t} \quad (23)$$

where $N =$ nutrient concentration, $C =$ algal concentration represented by cellular nutrient content, and $\mu =$ algal growth rate. The nutrient transport can be estimated by assuming a quasi-steady situation when the diffusive transport balances the uptake for algal growth. If a uniform uptake situation is assumed within the euphotic layer,

$$E\frac{\partial^2 N}{\partial z^2} = \mu C = \text{constant},$$

by prescribing the zero mass flux boundary condition

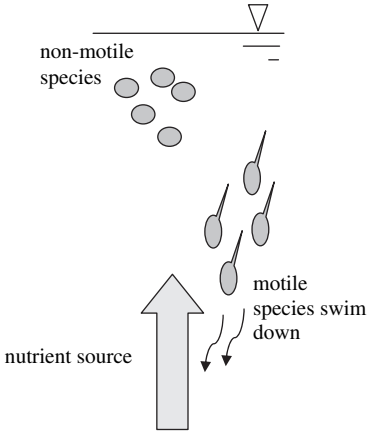

Fig. 10. Nutrient competition between motile and non-motile species.

$$\left(E\frac{\partial N}{\partial z}=0 \text{ at } z=0\right)$$

at the free surface, the nutrient mass balance can be solved resulting in a parabolic vertical nutrient profile:

$$N=(N_l-N_0)\frac{z^2}{l^2}+N_0 \tag{24}$$

where N_l, N_0 are the nutrient concentration at $z=0$ and $z=l$ respectively, and $N_0=N_l-(\mu C/2E)l^2$.

The nutrient mass flux into the euphotic layer therefore equals

$$E\frac{\partial N}{\partial z}_{(z=l)}=\frac{2E(N_l-N_0)}{l} \tag{25}$$

If the average algal concentration in the euphotic layer is denoted by C_N (in terms of cellular nutrient), the nutrient supply per unit algae then equals

$$\frac{2E(N_l-N_0)}{C_N l^2}$$

which cannot exceed (with $N_0=0$)

$$\frac{2EN_l}{C_N l^2} \tag{26}$$

Alternatively, the concentration profile can be assumed to be given by Eq. (3) (assuming nutrient unlimited situation). As an approximation, the time variation of nutrient concentration is assumed to be slow enough such that the nutrient mass flux can be estimated by assuming a quasi-steady mass balance:

$$E\frac{\partial^2 N}{\partial z^2}=K\mu e^{az-bl}(\beta\cos\ \beta z+a\sin\ \beta z)e^{kt} \tag{27}$$

Integrating, we have

$$E\frac{\partial N}{\partial z}=K\mu e^{-bl}e^{kt}e^{az}\ \sin\ \beta z+K_1 \tag{28}$$

where $K_1=0$ for zero mass flux at the surface. Integrating again, and noting that $a^2+\beta^2=\mu/E$, we have

$$\begin{aligned}N&=\frac{K\mu e^{-bl}e^{kt}e^{az}}{E}\left(\frac{a}{a^2+\beta^2}\sin\ \beta z-\frac{\beta}{a^2+\beta^2}\cos\ \beta z\right)+K_2\\&=K'e^{az}(a\sin\ \beta z-\beta\cos\ \beta z)+K_2\end{aligned} \tag{29}$$

where $K'=K\mu e^{-bl}e^{kt}$ can be treated to be a constant in a quasi-steady situation. With the nutrient concentration below the euphotic layer equals to N_l, the nutrient concentration profile is given by

$$\begin{aligned}N=K'\big[&e^{az}(a\sin\ \beta z-\beta\cos\ \beta z)\\&-e^{al}(a\sin\ \beta l-\beta\cos\ \beta l)\big]+N_l\end{aligned} \tag{30}$$

Our field data show that $a/\beta\ll 1$, and if we assume $al\ll 1$, Eq. (30) can be approximated by:

$$N=K'\beta(\cos\ \beta l-\cos\ \beta z)+N_l \tag{31}$$

A Taylor's expansion of the above nutrient profile would again result in an approximate parabolic profile, and the maximum nutrient supply to non-motile species given by Eq. (26) is recovered.

Using averaged values of $a=0.035\ \mathrm{m}^{-1}$, $\beta=0.29\ \mathrm{m}^{-1}$, $E=2.2\times10^{-4}\ \mathrm{m}^2\ \mathrm{s}^{-1}$, $l=6$ m, $v=1\ \mathrm{m\ day}^{-1}$ (see Table 3), the nutrient profiles computed using Eq. (30) and Eq. (24) are compared in Fig. 11. It can be seen that the nutrient solution can be reasonably approximated by a parabolic profile which can be conveniently used to estimate the diffusive nutrient flux into the photic zone.

From Eq. (26), it can be seen that the nutrient supply to non-motile species is governed by several factors—first, the strength of the nutrient source N_l; second, the strength of the turbulent diffusive transport E and the length of path l for which nutrient has to be transported; lastly, the amount of algae C_N sharing the nutrient supply. At low algal concentration, turbulent diffusion could be an effective means for nutrient transport. However, as the algal concentration increases, the supply per unit algal mass will be less. On the other hand, such kind of limitation does not exist for motile species. If C_N is chosen as the algal concentration level during bloom, it follows that if

$$\frac{2EN_l}{C_N l^2}<\mu' \tag{32}$$

it is more effective to rely on active migratory behaviour to harvest nutrient than on passive turbulent diffusion. In this sense, motile species may be considered to have a competitive advantage. Conversely, if

$$\frac{2EN_l}{C_N l^2}>\mu'$$

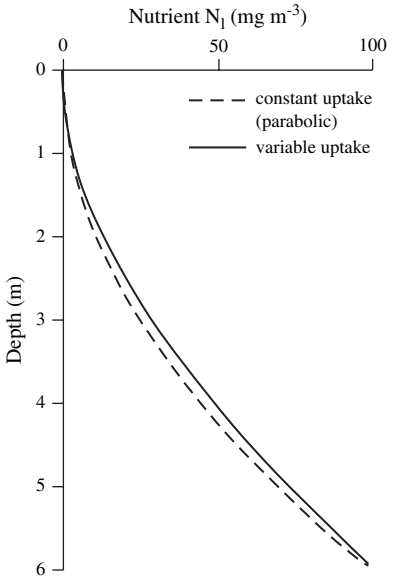

Fig. 11. Computed nutrient profile based on variable algal uptake (Eq. 30) and the parabolic approximation (constant uptake, Eq. 24) ($a=0.035\ \mathrm{m}^{-1}$, $\beta=0.29\ \mathrm{m}^{-1}$, $E=2.2\times10^{-4}\ \mathrm{m}^2\ \mathrm{s}^{-1}$, $l=6$ m, $v=1\ \mathrm{m\ day}^{-1}$; N_l and $N_0=100$ and 0 mg m^{-3}, respectively).

it will be expected that until the time of the bloom, non-motile species will be more competitive due to their fast growth rate. Therefore, a bloom of non-motile species will be formed instead.

Rearranging the inequality (Eq. 32), the threshold diffusivity for which motile species could have a competitive advantage over non-motile species is given by

$$E < \frac{\mu' l^2 C_N}{2N_l} \tag{33}$$

For typical values of $\mu' = 0.5\ \text{day}^{-1}, l = 6\ \text{m}, C_N = 100\ \text{mg m}^{-3}$ and $N_l = 200\ \text{mg m}^{-3}$ for Hong Kong waters, the criteria for motile species to become dominant is $E < 5.2 \times 10^{-5} \text{m}^2\ \text{s}^{-1}$. It is interesting to note that this is close to values reported by Margalef (1978)—diatoms predominate in regions of turbulence with $E = 2 \times 10^{-4}$ to $1 \times 10^{-2}\ \text{m}^2\ \text{s}^{-1}$; dinoflagellates predominate in regions of $E = 2 \times 10^{-6}$ to $1 \times 10^{-4}\ \text{m}^2\ \text{s}^{-1}$.

For given values of C_N, μ' and l, Eq. (33) is a hyperbolic relation between turbulence and nutrient level, and a diagram resembling Margalef's ''Mandala'' can be obtained (Fig. 12). Slow growing dinoflagellates will tend to dominate in the lower left hand region of the diagram where the turbulence and nutrient level are low. In this region, shortage of nutrient supply is the major factor hindering phytoplankton growth. Motility of dinoflagellates can enhance their nutrient harvesting capability in these environments (K-strategy). Fast growing diatoms (r-strategy), on the other hand, will be dominating in the upper right hand region of the diagram where turbulence and nutrient level are high.

Changing the values of μ', l and C_N (changing the type of dinoflagellates or the type of habitat) will shift the competition threshold towards the lower left or upper right corner. Increasing the dinoflagellate growth rate (faster growing dinoflagellates) will shift the threshold upper right since the dinoflagellates are more growth competitive. It is interesting to note that increasing light supply (increasing euphotic depth l) will also shift the threshold upper right. The increased competitive advantage of dinoflagellates due to increased l can be explained by the increased pathway nutrient has to be transported for uptake, and the increased euphotic layer depth sharing the same nutrient supply. This is similar to a shift from the energy deficiency, nutrient rich R region to the energy rich, nutrient deficiency S region in the Reynolds' ''Intaglio'' with a change from diatom to dinoflagellates dominancy and *vice versa*. The fact that dinoflagellates could have higher competitive advantage in clear waters may be one of the factors contributing to more dinoflagellate activities in the pristine northeastern waters in Hong Kong (Lee et al., 2005). In order to have a bloom, the nutrient level has to be higher than a threshold level (see next section). This gives rise to a void area in the bottom right portion of the diagram. Moreover, in order to have a bloom, the water column has to be stable enough following the stability criteria. Therefore, the diagram cannot extend infinitely but has to be bounded at the right hand side.

The above heuristic model provides a quick insight into the roles played by various factors in shifting algal bloom from

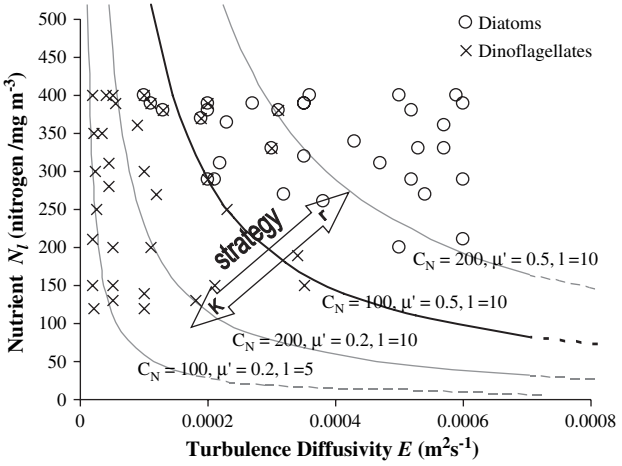

Fig. 12. Nutrient competition between diatoms and dinoflagellates: numerical prediction for diatom (circles) or dinoflagellate (crosses) dominance (for $C_N = 100\ \text{mg m}^{-3}, \mu' = 0.5\ \text{day}^{-1}, l = 10\ \text{m}$) shown against analytical criterion (solid line, Eq. 33).

diatoms to dinoflagellates, and *vice versa*, based on nutrient harvesting. A surprising implication from the diagram is the dependence of the competition threshold on the algal concentration during a bloom, C_N. Normally, the blooming level C_N is defined against a normal background level; when the algal concentration is much higher than the background level (say by an order of magnitude), it would be considered as a bloom (Smayda, 1997b; Wong, 2004). In eutrophic waters, the background of algal concentration is higher and hence also for the blooming level C_N. It is more difficult for diatoms to achieve further higher concentration as they are more prone to self-limitation (nutrient limitation and self-shading) than dinoflagellates. This may partly explain the sharp increase in number of dinoflagellate blooms compared to diatom blooms in recent decades due to increasing eutrophication (Hallegraeff, 1993; Anderson, 1994).

The foregoing analytical result on species competition in terms of nutrient harvesting has been checked against numerical solution of the full advective diffusion equations for the case with $\mu' = 0.5\ \text{day}^{-1}$, $l = 10\ \text{m}$ and $C_N = 100\ \text{mg m}^{-3}$ (Wong and Lee, 2006a). The model is initialised with a uniform vertical distribution of diatoms and dinoflagellates, $C(z, 0) = C_N/10$, and run for 10 days. This time period would be sufficient for even the slow growing dinoflagellates (that double every two days) to bloom. If the species concentration increases by an order of magnitude to C_N, a bloom is assumed to occur. Nutrient is assumed to be supplied solely from the sea bed with initial concentration of $0\ \text{mg m}^{-3}$ in the photic zone and N_l in the lower layer. Monod growth with half saturation constant of $10\ \text{mg m}^{-3}$ is assumed for diatoms. Cell quota type of growth (Droop, 1973) is assumed for dinoflagellates, with parameters converted from the Monod growth model (Wong, 2004). A constant mortality rate of $d = 0.1\ \text{day}^{-1}$ is assumed. Dinoflagellates are assumed to swim in a diel cycle to the water surface and the bottom of the euphotic layer (upward between 6 am–6 pm,

and downward between 6 pm–6 am). Ascending and descending motion cease when the algae reached the top and bottom of the euphotic layer respectively.

A FTCS Eulerian scheme is used to solve the governing equations for the diatoms and nutrient ($\Delta t = 60$ s, $\Delta z = 1$ m), while a Lagrangian particle scheme is used to simulate the swimming behaviour of dinoflagellates (Wong and Lee, 2003; Wong, 2004). For the above stated conditions of $\mu' = 0.5\ \text{day}^{-1}$, $l = 10$ m and $C_N = 100\ \text{mg m}^{-3}$, the model can be run for every point on the nutrient–turbulent diffusivity (N_l, E) diagram; for each run, the dominance of either diatoms or dinoflagellates can be predicted. The model is run for a wide range of parameters (diatom growth rate $\mu = 1.5$–$2\ \text{day}^{-1}$; diffusivity $E = 0.2$–$6 \times 10^{-4}\ \text{m}^2\ \text{s}^{-1}$; bottom nutrient concentration $N_l = 120$–$400\ \text{mg m}^{-3}$; dinoflagellate migration speed $= 0.5$–$2\ \text{m h}^{-1}$; diatom sinking velocity $=$ 0–1 m day^{-1}). The numerical result shows that the analytical threshold value based on heuristic reasoning (Eq. 33, shown as solid line) can generally give a reasonable prediction of the species competition between diatoms and dinoflagellates (Fig. 12). It is worth noting that if the nutrient concentration is extremely high, nutrient supply will be unlimiting to both diatoms and dinoflagellates and there is little necessity for competition. In that case, even if the diffusivity is above the competition threshold, dinoflagellates will still grow beyond the blooming level (although, with diatoms dominating). It is also observed that the diatom growth rate plays little role in the competition as long as it is much greater than the dinoflagellate growth rate. Similar model runs have also been made with other combinations of μ', l and C_N (not shown). In general, the results show that the competition threshold can reasonably predict the winner of the competition.

The reader is reminded that the above simple heuristic model provides only a quick insight on dominancy between motile and non-motile species. The real situation is much more complicated—both in regard to nutrient supply and assimilation, and the eco-physiological responses to environmental factors. The actual problem for species selection involves competition for light (or self shading effect), selective grazing, aggregation to the optimal depth, growth regulation by nutrient ratios such as N:P and Si:P (Hodgkiss and Ho, 1997) and various other factors (Watanabe et al., 1995).

3.5. Threshold nutrient level

Anthropogenic nutrient input is generally believed to be the major causative factor for the large number of algal blooms in recent decades. Studying the long-term water quality data in Hong Kong, Hodgkiss and Ho (1997) observed a sharp increase in number of algal blooms whenever the nitrogen level rose above 100 mg m^{-3} and phosphorus level rose above 20 mg m^{-3}. From a material conservation point of view, for an increase in biomass, there must be a corresponding supply in material for cell formation. In a closed system if all nutrient inputs are converted into algal biomass, 1 mg input will correspond 1 mg increase in biomass. For a typical nitrogen to chlorophyll-*a* ratio of 10, phosphorus to chlorophyll-*a* ratio of 1.5, and chlorophyll-*a* concentration of 10 mg m^{-3} during algal blooms in Hong Kong waters, the required nitrogen and phosphorus input are 100 mg m^{-3} and 15 mg m^{-3} respectively. Surprisingly, these values are close to the threshold level reported by Hodgkiss and Ho.

If the water column is not closed, with nutrient transported up the water column from sea bed and algal biomass lost from below the euphotic layer, the vertical transport equations have to be considered. From Eq. (25), the nutrient mass flux is given by (with $N_0 = 0$),

$$\frac{2EN_l}{l}$$

On the other hand, the biomass production due to algal growth equals

$$\mu C_N l$$

By mass conservation, the algal production (in terms of nutrient) has to be less than the material supply, thus

$$\mu C_N l < \frac{2EN_l}{l}$$

Recall that in order to have a bloom, the turbulent diffusivity has to be below the critical threshold (inequality 14), therefore

$$\mu C_N l < \frac{8\mu l N_l}{\pi^2}$$

$$N_l > \frac{\pi^2}{8} C_N \tag{34}$$

The threshold level for nitrogen and phosphorus thus obtained are 120 mg m^{-3} and 18 mg m^{-3} respectively. The above again suggests that the minimum required nutrient level exists, and is of the order of C_N. The heuristic result (Eq. 34) can serve as a rough guide for threshold nutrient level required for algal blooms. The reader is reminded that in reality, the cell composition and nutrient requirement vary from species to species, and the above threshold nutrient level also depends on the algal concentration to be defined as a bloom. Moreover, it is not always necessary for nutrient to be supplied by mass transport from the sea bed. For the case of dinoflagellates, they can even swim down to the sea bed to fetch nutrients. However, the material conservation argument and hence the approximate nutrient threshold remains applicable.

An additional consideration for the nutrient threshold of dinoflagellate blooms could be the modification of migratory behaviour by nutrient availability. From our field observations, dinoflagellate cells in samples collected during blooms appear to be swimming more actively. This is consistent with the observation by Cullen and Horrigan (1981) in their experiment that vertical migration ceases when nutrient becomes depleted. However, further studies would be necessary to resolve these complexities of dinoflagellate blooms.

3.6. Simple model for bloom forecast

Based on the foregoing theoretical results, a decision model can be constructed to predict the likelihood of algal blooms (Fig. 13):

- First, a representative vertical turbulent diffusivity E for the region under consideration is estimated (see next section). The estimated value of E has to be checked against the stability criteria given by Eqs. (15) and (22). If the stability criteria are fulfilled, the water column is sufficiently stable for bloom formation (for Hong Kong waters, checking on the non-motile stability criteria alone may be sufficient since diatoms blooms are always observed in more turbulent waters).
- Second, check whether the nutrient level N_l has exceeded the threshold level, especially for prolonged period. If yes, there is sufficient nutrient to support the formation of algal bloom and a bloom would likely occur. On the other hand, prolonged low nutrient concentration would definitely suggest insufficient material source for growth, and further checking is then unnecessary.
- Lastly, to predict the type of bloom (motile or non-motile species), the competition threshold (Eq. 33) has to be checked. When the diffusivity E is below the threshold value $\mu' l^2 C_N/2N_l$, a bloom would likely be composed of motile species.

4. Model application and parameter estimation

The foregoing model assumes constant values for the algal growth and sinking rate, and the vertical mixing coefficient. It is recognised that this is a highly idealised representation aimed to develop a simple analytical framework for bloom forecasts. In practice algal growth rate changes with depth (e.g. due to light extinction); the vertical diffusivity also varies in accordance with distance from the free surface or bottom. Consistent with the spirit behind this first-order theory, in model application the depth-averaged values are used for the parameters wherever appropriate. Similarly, the parameters are also time-averaged over the photo-period. For the threshold nutrient levels, 120 mg m^{-3} is taken for nitrogen and 18 mg m^{-3} taken for phosphorus for Hong Kong waters, based on the semi-empirical approach and past field observations (Section 3.5). The nutrient supply concentration N_l, on the other hand, is taken as the maximum level for the limiting nutrient (nitrogen in our examples below) measured at the field station preceding the bloom. Other model parameters are estimated as follows:

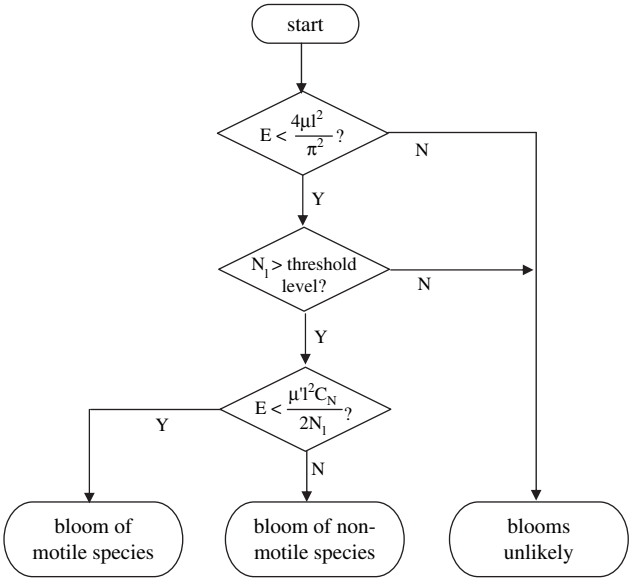

Fig. 13. Algal bloom forecast model using the vertical stability theory.

4.1. Euphotic depth l

The euphotic depth l can be estimated from the Secchi depth or light attenuation measurement. Based on past field and modelling works (Lee and Lee, 1995), we assume Steele's equation for light limitation (see e.g. Thomann and Mueller, 1987),

$$G_I = \frac{I}{I_s}\exp\left(1-\frac{I}{I_s}\right) \tag{35}$$

where I_s is the saturating light intensity and is taken to be the irradiation just below the water surface. The euphotic depth is defined as the depth at which the light limitation $G_I = 0.1$ ($I/I_s = 0.04$). Adopting the Beer-Lambert's Law for light attenuation, $I = I_s \exp(-\gamma z)$, where γ is the light attenuation coefficient, the euphotic depth can be estimated with

$$l = 3.2/\gamma$$

In case only Secchi depth (z_s) measurements are available, an empirical relation can be used to relate the light attenuation coefficient to Secchi depth, $\gamma = 1.7/z_s$ (Thomann and Mueller, 1987), resulting in

$$l = 1.9 z_s$$

4.2. Algal growth rates μ and μ'

The algal growth rate can be obtained from measurements on algal cultures of representative species. In the absence of measurements, it can be obtained from literature values and the effect of temperature estimated using a temperature growth function (e.g. Thomann and Mueller, 1987)

$$\mu(T) = \mu_0 G_T(T) = \mu_0 (1.066)^{T-20^oC}$$

where μ_0 is the maximum algal growth rate. Due to light attenuation, the growth rate for non-motile species decreases with depth. For the non-motile species, the depth-averaged growth rate over the euphotic layer is then given by ($l = 3.2/\gamma$):

$$\overline{\mu} = \frac{1}{l}\int_0^l \mu_0 G_I G_T \, dz \approx 0.5\mu_0 G_T \tag{36}$$

The net growth rate can then be obtained by

$$\mu = 0.5\mu_0 G_T - d = 0.5\mu_0(1.066)^{T-20^oC} - d \quad (37)$$

where d is the algal loss rate due to mortality and flushing. Typically, $\mu_o = 2$ day^{-1} for diatoms (Jorgensen, 1979; Bowie et al., 1985); $d \approx 0.1\mu_0$ is often assumed. The net growth for the motile species can be similarly estimated, with $\mu_0' = 0.5$ day^{-1}; the depth-averaging process is however not necessary for motile species since they tend to aggregate into a thin layer of optimal light intensity ($\mu' = \mu_0'(1.066)^{T-20^oC} - d$).

Although the effect of nutrient on algal growth has not been included in estimating the growth rate, with the threshold nutrient levels considerably higher than the half-saturation constants (around 15 mg m^{-3} and 2 mg m^{-3} for nitrogen and phosphorus respectively; see e.g. Lee and Lee, 1995), an optimal nutrient-growth relationship is automatically implied.

4.3. Sinking and migration velocities

In developing our bloom prediction model, the sinking and migration velocities turn out to be unimportant in the final stability criterion. This is based on the observed values of the migration and sinking velocity during the bloom events. From the field data, the migration speed of motile species is estimated directly from the speed of advance of the thin concentrated layer of dinoflagellates. Table 1 shows the values estimated for the blooms caused by motile species in Kat O.

The sinking velocity of non-motile species is estimated from the rate of change of the centre of gravity of the vertical algal distribution during the dark period (Fig. 14). If the loss rate is assumed to be constant with depth, it would have no effect on the shape of concentration profile and centre of gravity. The effect of water turbulence mainly serves to smooth the concentration profile. Therefore, the average downward movement (i.e. the rate of change in centre of gravity) can be considered to be caused by sinking alone. As an illustration, the change in centre of gravity of biomass during the bloom in late Aug2000 is shown in Fig. 14. Sinking velocity is calculated to be within 1.2–1.8 m day^{-1}. This lies well within the general reported range of a few tens of centimetres to several meters per day for marine diatoms (Smayda, 1970; Jorgensen, 1979). Table 2 shows a summary of sinking velocity estimated from diatom blooms occurring in Lamma Island together with a comparison with literature values for similar species.

Table 1
Migration speeds for motile species obtained from field data. Literature values for similar species from Cullen and Horrigan (1981), Levandowsky and Kaneta (1987) and Watanabe et al. (1995)

Period	Causative species	Migration speed (m h^{-1})	
		This study	Literature
19–21 Feb 2000	Mixed species	1.0	–
16–18 Mar 2000	*Akashiwo sanguinea*	0.4–1.0	1.1
02–08 May 2000	*Prorocentrum sigmoides*	0.5–1.0	0.36–0.9
21–25 Mar 2001	*Gonyaulax polygramma*	1.0–2.0	1.8
14–23 Apr 2001	*Chattonella ovata* & *Dictyocha speculum*	0.7–1.0	0.8
29 Apr–02 May 2001	*Chattonella ovata* & *Dictyocha speculum*	0.7	0.8

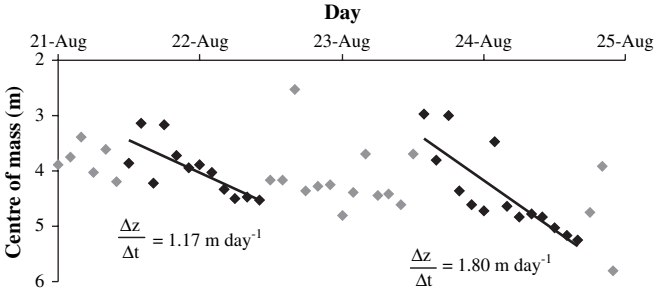

Fig. 14. Time variation of centre of mass (m below surface) of algal profile (August 2000, Lamma Island).

4.4. Estimation of vertical mixing

To apply the vertical stability theory, an estimate of the vertical turbulent diffusivity E representative of the semi-enclosed tidal inlet is required. Vertical mixing is related directly to the strength of tidal current and the vertical density stratification. A simple relation to estimate the vertical diffusivity as a function of readily available parameters can be derived from three-dimensional tidal circulation models and well-established semi-empirical laws of wind-driven currents. The method is illustrated using Kat O as an example.

4.4.1. Computation of tidal circulation and flushing

Kat O is featured by a cluster of islands including Kat O Chau, Tui Min Chau, Crescent Island (Fig. 1). It has two eastward openings separated by Tui Min Chau, and joins Double Haven, a protected marine reserve area, to the south. The water depth varies from about 6 m at the southern end to 13 m at the northern end, where the O Pui Tong fish culture zone (FCZ) is located. The tidal circulation in Mirs Bay including Kat O and Tolo Harbour has been modelled using the Environmental Fluid Dynamics Computer Code (EFDC) (Hamrick, 1992); the open boundary is located at the entrance to Mirs Bay (Fig. 1). The entire model has a total of 8709 grid cells; the grid size ranges from 75 to 450 m. The model has been extensively tested against analytical solutions of long wave

Table 2
Sinking velocity estimated from diatom blooms in Lamma Island. Literature values for similar species from Smayda (1970)

Period	Causative species	v (m day^{-1})	
		Observed	Literature
10–11 Aug 2000	Mixed diatoms	0.6–2.5	–
18–24 Aug 2000	Mixed diatoms	1.2–1.8	–
16–20 Jun 2001	*Thalassiosira subtilis*	0.6–1.1	0.39–2.10
20–26 Jun 2002	*Skeletonema costatum*	0.7–1.2	0.30–1.35
01–06 Jul 2002	*Skeletonema costatum*	0.6–0.7	0.30–1.35
24 Jul 2002	*Chaetoceros* spp.	0.6–0.8	0.53–0.85
12 Aug 2003	*P. pseudodelicatissima*	0.2–0.5	0.35–0.5

Table 3
Algal growth and stability parameters at Kat O and Lamma Island during bloom events (Distance between surface and bottom (Δz) for Lamma Island and Kat O are 6 m and 4 m respectively)

	Period	N_l (mg m^{-3})	z_s (m)	l (m)	μ (day^{-1})	μ' (day^{-1})	$4\mu l^2/\pi^2$ (m^2 s^{-1})	$\mu' l^2 C_N/2N_l$ (m^2 s^{-1})	Temperature (°C)		Salinity (ppt)		$\Delta\rho/\Delta z$ (kg m^{-4})	W_{10} (m s^{-1})	U (cm s^{-1})	U_s (cm s^{-1})	Ri	E (m^2 s^{-1})	ν (m day^{-1})	a (m^{-1})	β (m^{-1})
									Surface	Bottom	Surface	Bottom									
Diatom blooms (Lamma Island)	10–11 Aug 2000	202	2.4	4.6	1.3	0.7	1.2e-4	5.0e-5	28.2	25.9	29.0	33.7	0.71	2.4	6.3	14.3	33.2	9.5e-5	1.6	0.098	0.379
	18–24 Aug 2000	191	4.8	9.1	1.2	0.7	4.7e-4	2.0e-4	27.1	25.6	28.9	30.2	0.24	2.9	7.0	16.7	8.2	3.1e-4	1.5	0.028	0.209
	16–20 Jun 2001	326	2.6	4.9	1.2	0.7	1.4e-4	3.5e-5	27.0	25.7	20.4	27.2	0.91	2.9	3.8	13.1	50.8	1.3e-4	0.9	0.041	0.327
	20–26 Jun 2002	323	2.9	5.5	1.3	0.8	1.9e-4	4.9e-5	29.0	27.1	25.7	30.1	0.65	4.0	3.6	16.1	23.8	2.9e-4	1.0	0.020	0.232
	01–06 Jul 2002	513	3.2	6.1	1.3	0.7	2.2e-4	3.6e-5	27.8	26.3	23.2	27.0	0.56	3.1	7.7	18.0	16.5	1.7e-4	0.7	0.024	0.294
	24 Jul 2002	162	2.8	5.4	1.3	0.7	1.7e-4	9.0e-5	28.1	26.7	26.2	28.1	0.31	3.1	9.1	19.7	7.6	4.3e-4	0.7	0.009	0.186
	12 Aug 2003	244	3.5	6.6	1.3	0.7	2.7e-4	9.2e-5	28.5	27.4	29.2	31.5	0.35	2.1	7.6	15.0	14.8	8.9e-5	0.4	0.026	0.414
Blooms caused by motile species (Kat O)	19–21 Feb 2000	188	3.8	7.2	0.7	0.4	1.7e-4	7.4e-5	17.8	17.5	31.8	31.8	0.02	1.5	1.5	6.0	5.5	7.5e-5			
	16–18 Mar 2000	234	6.1	11.6	0.7	0.4	4.6e-4	1.6e-4	19.2	18.2	30.7	30.9	0.10	1.5	0.9	5.6	30.1	2.0e-5			
	02–08 May 2000	575	5.2	9.9	1.0	0.6	4.6e-4	6.6e-5	24.8	22.3	28.9	30.5	0.48	1.8	0.8	6.3	114.9	2.9e-5			
	21–25 Mar 2001	228	4.6	8.7	0.8	0.5	3.0e-4	1.1e-4	21.7	19.9	31.6	31.6	0.10	2.1	0.9	7.4	17.5	4.6e-5			
	14–23 Apr 2001	225	5.6	10.6	0.9	0.5	4.7e-4	1.7e-4	21.8	21.5	32.2	32.4	0.05	1.8	0.9	6.5	12.4	3.9e-5			
	29 Apr–02 May 2001	482	8	15.2	1.0	0.6	1.1e-3	1.9e-4	24.7	22.4	31.9	32.1	0.21	2.0	1.1	7.1	39.2	3.8e-5			

propagation, and has also been validated against field measurements of the flow field at representative tidal states. The spatial distribution of tidal velocities is obtained by Acoustic Doppler Current Profiler (ADCP) measurements taken from a moving vessel along a circuit around the bay. Fig. 15 shows the comparison of the computed depth-averaged instantaneous peak ebb current field in Kat O with the ADCP measurements taken over about 70 min in a 26-h dry season survey. The circulation in Kat O region is mainly governed by the flow going in and out of Double Haven. During flood tide, current flows into Double Haven through Kat O and *vice versa* during neap tide. The highest velocity is observed at the narrow deep pass between Kat O Chau and Crescent Island (position A, Fig. 1). The observed flow speeds are quite similar at positions around the main entrance into O Pui Tong, with a maximum of about 10 cm s^{-1}. Supported by the measurements, the velocity inside the bay is generally low and near measurement threshold, and varies from 4–6 cm s^{-1}. Fig. 16a) shows the comparison of computed and measured longitudinal (along channel) velocity in the deep pass joining Double Haven and Kat O. The computed tidal current inside O Pui Tong is found to be in the order of 1 cm s^{-1} or less, which is also consistent with the field data. In general the main computed features are in reasonable agreement with the observations.

Tidal flushing of the inner Kat O bay is also determined using a numerical tracer technique (Choi and Lee, 2004). A hypothetical conservative pollutant of unit concentration is introduced in the inner bay (O Pui Tong) at $t = 0$; the subsequent change of the tracer mass is computed by solving the tracer transport equation, from which the flushing time can be determined. The flushing rate (the inverse of flushing time) of inner Kat O bay has been determined to be 0.025 day^{-1}. It is much smaller than the typical net algal growth rate which is of the order of 1 day^{-1}—suggesting the possibility of bloom development within the bay. The weak tidal exchange between the bay and outside waters also justifies the prediction of algal blooms based on biomass development in the water column. A similar calculation is done for Lamma Island. Further details can be found in Wong (2004).

4.4.2. Correlation of tidal range and current

With the tidal circulation computed, here we aim at developing a simple and robust method to estimate the representative tidal current of the study area on any given day. As tides in Hong Kong are mixed and mainly semi-diurnal, the tidal current characteristic in the bay can be estimated with M2 tidal forcing. The tidal current for the semi-enclosed bay is first computed by the circulation model under M2 tidal forcing with different tidal ranges. A tidal current for the bay is calculated by averaging the magnitude of tidal current in all grid cells lying within the bay (e.g. for Kat O, the shaded region in Fig. 1). The maximum value of this spatially-averaged current over the tidal cycle is used to represent the tidal velocity at that tidal range. Lastly, by plotting these representative tidal currents with the tidal range, a relationship between the tidal current and tidal range is obtained. Given the tidal constituents for a particular place (e.g. as obtained from an extended

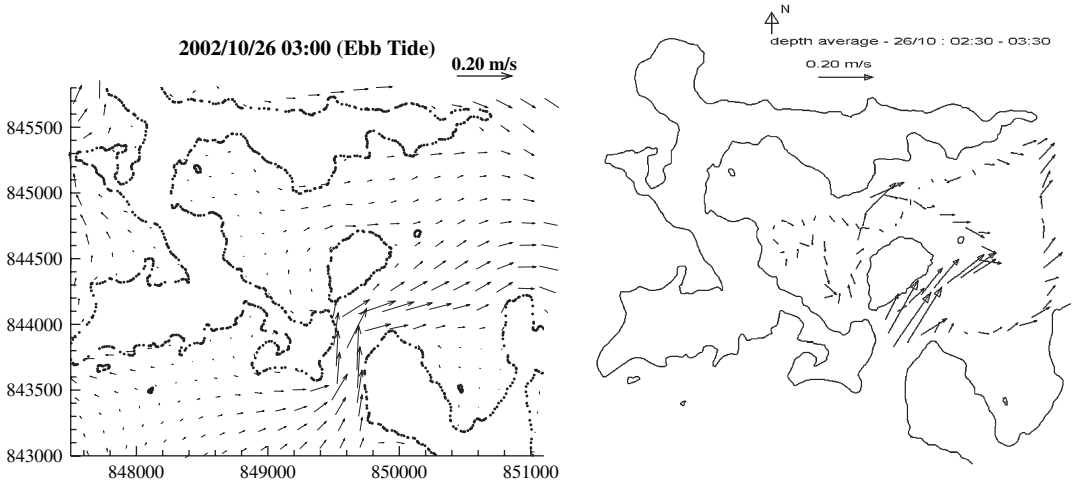

Fig. 15. Comparison between predicted and observed tidal circulation in Kat O in dry season (left, predicted ebb tide; right, observed ebb tide).

harmonic analysis of a long-term record), the tidal range for any particular day can be readily predicted. Therefore, a quick estimate of the tidal current can be easily obtained without the necessity to run the hydrodynamic model every time. This simplified method gives predictions that are supported by field data, and is commensurate with the complexity of the ecological problem at hand. The results of the circulation model suggests an approximately linear relation between tidal current and tidal range (Fig. 16b), and the representative tidal current at the two sites (Kat O and Lamma Island respectively) can be estimated as:

$$U\ \left(\mathrm{m\ s^{-1}}\right) = 0.041\Delta H + 0.009 \tag{38}$$

$$U\ \left(\mathrm{m\ s^{-1}}\right) = 0.0067\Delta H + 0.0015 \tag{39}$$

where ΔH is the tidal range of the day. In general, surface wind would also have a considerable effect on the surface current. The effect is generally considered as a surface shear or as a surface tidal current of a certain fraction of the wind speed. The wind driven current is assumed to be related to the wind speed by the 3% rule (Bowden, 1983; Lewis, 1997):

$$u_w = 0.03W_{10}$$

where W_{10} is the average wind speed at 10 m height during the period concerned.

The surface current is made up of two contributions: the effect of tidal current and the wind. Assuming a one-seventh power law also for the tidal current, the surface current at the study sites (Kat O and Lamma Island respectively) are given by

$$U_s\left(\mathrm{m\ s^{-1}}\right) = 0.0077\Delta H + 0.0017 + 0.03W_{10} \tag{40}$$

$$U_s\left(\mathrm{m\ s^{-1}}\right) = 0.047\Delta H + 0.010 + 0.03W_{10} \tag{41}$$

For a typical tidal range of 1.7 m, wind speed of 2 m s^{-1} at the measurement level, typical surface current at Kat O is around 9 cm s^{-1}. For a typical tidal range of 1.7 m, wind speed of 3 m s^{-1} at the measurement level, typical surface current at Lamma Island is around 20 cm s^{-1}. These predicted values generally match well the direct velocity measurements at the two study sites.

4.4.3. Vertical diffusivity

The vertical turbulent diffusivity is estimated using (a) the tidal current prediction given in the previous section and (b) a well validated semi-empirical formula to account for wind effect and damping of turbulence by density stratification. Based on studies in the Irish Sea, James (1977) has provided the following empirical equation for estimating the turbulent diffusivity in a water column of uniform density

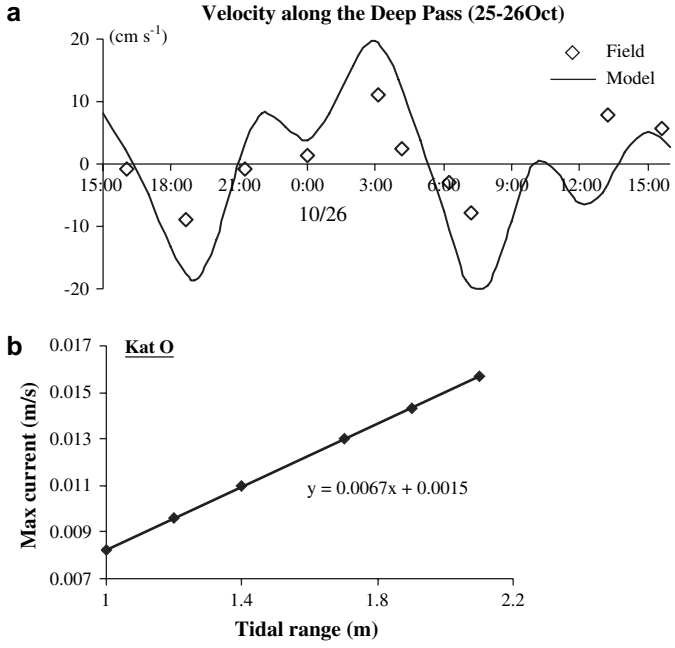

Fig. 16. (a) Comparison of predicted and measured tidal current at Point A (Deep Pass) in dry season. (b) Maximum tidal current in O Pui Tong against tidal range (M2 tide).

$$E = 1.59 \times 10^{-3} UH + 4.3 \times 10^{-4} W_{10}^2 \quad (W_{10} > 4.2)$$

$$E = 1.59 \times 10^{-3} UH + 1.02 \times 10^{-4} W_{10}^3 \quad (W_{10} < 4.2) \qquad (42)$$

In the presence of density stratification, the turbulent diffusivity will be reduced by the damping effect of body force. The amount of such a reduction could be related to the gradient Richardson number

$$Ri = \frac{g}{\rho}\frac{\partial \rho}{\partial z} \Big/ \left(\frac{\partial u}{\partial z}\right)^2$$

(Fischer et al., 1979; Bowden, 1983). The well-validated relationship by Munk and Anderson (1948) is used,

$$E = \frac{E_0}{(1 + \alpha Ri)^{\beta}} \qquad (43)$$

where E_0 is the turbulent diffusivity estimated for unstratified conditions; α and β are empirical constants taken to be 0.5 and 1.5 respectively. Such a parametric relation to account for reduction of turbulence by density stratification has been found to be adequate to describe the predominantly horizontal tidal flows in Hong Kong's coastal waters. Vertical salinity profiles predicted by such a simple turbulence closure are found to agree satisfactorily with field measurements. The velocity gradient, on the other hand, is rather difficult to measure especially in semi-enclosed shallow waters where the current can be very weak and near measurement threshold. In addition, very often, salinity and temperature measurements are available at 2–3 depths only. Therefore, a bulk Richardson number is used,

$$Ri = \frac{\Delta \rho}{\Delta z}\frac{gH^2}{\rho U_s^2}$$

where Ri is the bulk Richardson number (an upper bound of $Ri \leq 15$ is set in using Eq. 43); U_s is maximum surface current of the day, Δz is the vertical distance between surface and bottom measurement levels, and H is the mean water depth. Based on the measured wind and predicted tidal range, a representative value of E can hence be obtained for any day for Kat O and Lamma Island. More details on the diffusivity estimation, including the development and validation of the hydrodynamic models, can be found in Wong (2004).

5. Application to field data

5.1. Validation with bloom events

Over the 2000–2003 period, 21 blooms were observed at the two field stations. Out of these, 8 blooms are caused by the non-chlorophyll bearing species *Noctilluca* (hence not detectable by our chlorophyll fluorescence measurements). The simple algal bloom forecast model is tested using the field data of seven diatom bloom occurrences observed in Lamma Island and six bloom occurrences caused by the motile species (dinoflagellates plus *Chattonella ovata*) in Kat O (Lee et al., 2005). For each bloom event, the algal growth and water column stability parameters are estimated from field measurements immediately prior to the bloom. Table 3 shows a summary of the estimated parameters. It can be observed that the nutrient (total inorganic nitrogen) levels prior to these blooms are higher than the threshold level. The values of estimated vertical diffusivity E are plotted against the stability criteria $4\mu l^2/\pi^2$ (Eq. 15) in Fig. 17, and against the competition threshold $\mu' l^2 C_N / 2N_l$ (Eq. 33) in Fig. 18, where predicted values of μ and μ' (Eq. 37) are used. It can be seen that for the bloom events, the vertical turbulent diffusivity determined from the observed wind speed, density gradient and the tidal range, is generally less than the bloom criteria (Fig. 17). Small violation for the bloom occurring in July 2002 may be explained by the fact that the bloom was forming slowly (almost in steady state). As shown in Fig. 18, all the diatom bloom data fall within the upper region, while the dinoflagellate bloom data fall below the competition threshold. As an independent check, the model has also been applied to a dinoflagellate bloom caused by *Prorocentrum micans* in Kat O in August 2004, and five bloom events (two diatom and three dinoflagellate blooms) in two tidal inlets (Yim Tin Tsai, YTT; Yung Shue Au, YSA) in Tolo Harbour (Fig. 1). Again, the model is in agreement with the field data. Overall, it can be observed that the bloom forecasts for both non-motile and motile species are well-supported by the field data.

5.2. Algal bloom forecast for Lamma Island and Kat O (2000–2003)

To further test the validity of the theory, the model is applied to the 4 years (2000–2003) of continuous monitoring data in Lamma Island and Kat O (Fig. 19). The shaded regions in the graph indicate times when the nutrient concentration is higher than the threshold level. The red line represents the stability criteria. The black line joining the crosses represents the estimated vertical diffusivity. For an algal bloom to occur, two conditions should be fulfilled. First, the nutrient concentration

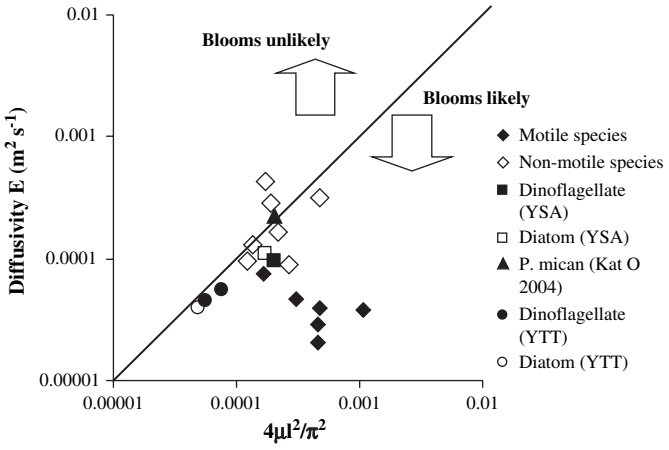

Fig. 17. Comparison of algal bloom occurrence with prediction using stability criterion (Eq. 15).

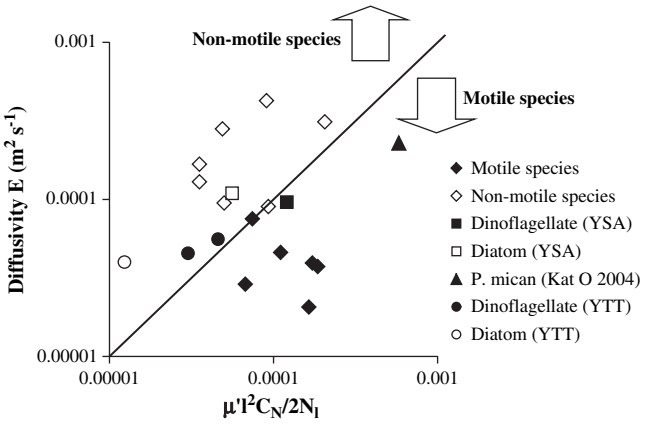

Fig. 18. Comparison of bloom occurrence of motile and non-motile species with prediction from competition threshold (Eq. 33).

must be above the threshold (i.e. in the shaded regions). Nutrient sources can be due to sewage outfalls, stormwater pollution or terrestrial runoff, riverine input, rainfall, or regeneration at sea bed. Second, if the diffusivity drops below the stability threshold, the water column is sufficiently stable, and a bloom may develop in the weak-flushed water.

In Fig. 19a, it can be observed that in Lamma Island, the nutrient level is generally higher than the threshold level, except in some dry season months (October to March). This suggests that nutrients are rarely limiting for bloom formation in this area. However, due to strong water turbulence (and high turbidity, i.e. smaller euphotic depth which reduces the value for stability criteria), algal blooms tend to occur only during the wet season when the water column is stratified and sufficiently stable. This prediction agrees well with the times when algal blooms are observed in Lamma Island (indicated by the arrows). In this area, strong turbulence and shallow euphotic layer are the main limiting factors for bloom formation; an algal bloom is normally only observable in the summer wet season. The blue line in the figure represents the competition threshold. It can be observed that the diffusivity is always above the competition threshold. Therefore diatoms will always have competition advantage regardless of where the nutrient comes from. This may also explain why dinoflagellate blooms are uncommon in Lamma Island.

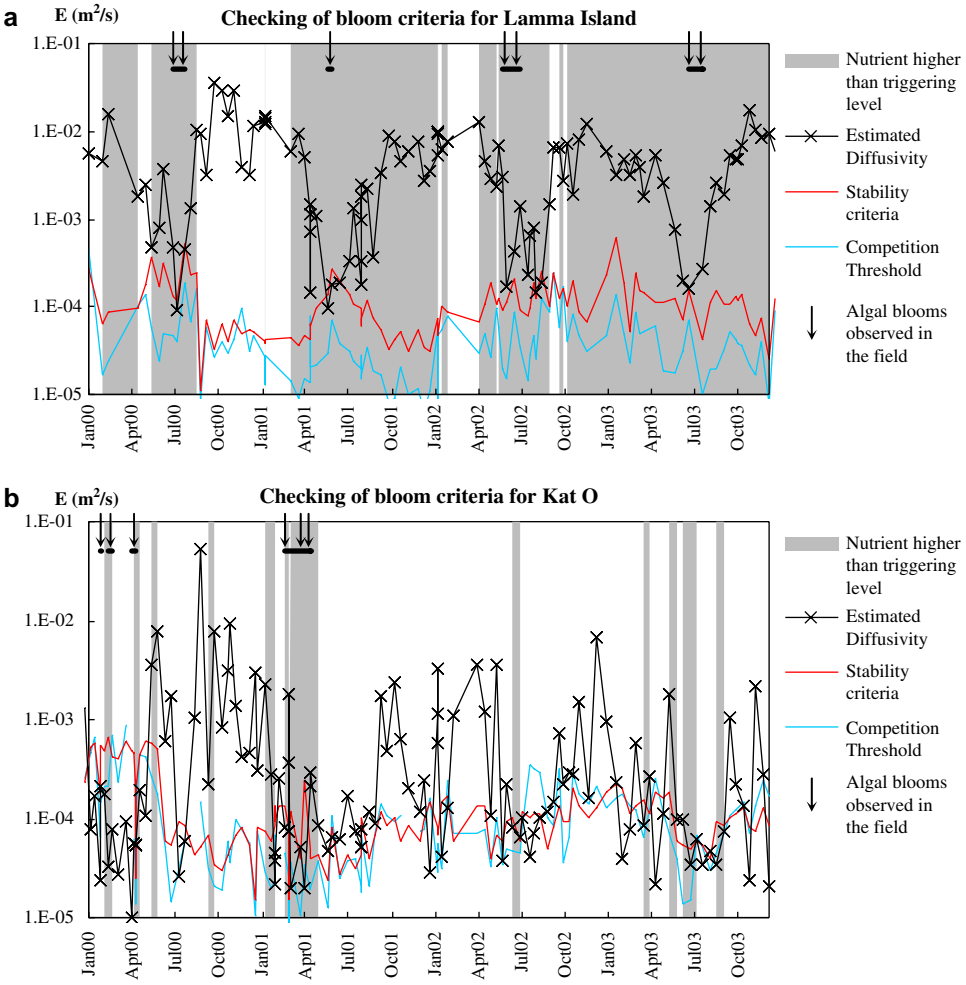

Fig. 19. Comparison of predicted and observed bloom occurrence (2000–2003) for (a) Lamma Island; (b) Kat O (minor blooms caused by *Noctiluca scintillans* and similar species without obvious chlorophyll signal are not shown).

The situation is more complicated in the relatively nutrient-poor northeastern waters (Kat O). As observed in Fig. 19b, both the nutrient and water stability play important roles in the bloom formation. Due to the weaker tidal currents in Kat O, the turbulent diffusivity is often below the stability criteria, especially under the typically low wind conditions in March to May. It is also interesting to note that some blooms occur in the absence of any vertical stratification (see also Table 3). At this location, the nutrient level is relatively low. Detritus decomposition at the sea bed plays an important role in the nutrient regeneration and supply. Algal blooms could only occur whenever the nutrient level becomes higher than the threshold level. Moreover, with vertical diffusivity below the competition threshold (blue line), the bloom of dinoflagellates is favoured. Once a bloom develops, nutrient depletion would occur. It is under these conditions that dinoflagellates have a competitive advantage over diatoms, by swimming down to near bottom to fetch nutrients at night, and up towards the surface during the day to obtain energy.

From summer 2001 onward, there has been a drop in the nutrient level in the area, reflecting a general decrease in pollution loading into Tolo Harbour and Mirs Bay (Fig. 1); red tides also became rare. Fig. 19b predicts the possibility of red tides in summer 2003; unfortunately due to equipment malfunctioning, accurate nutrient data to check this prediction are not available during this period. In general, the model predictions of bloom occurrences agree reasonably well with observations.

6. Concluding remarks

Hydrodynamics and algal dynamics are closely linked. First, in a semi-enclosed bay, material exchange with the open sea relies on tidal flushing. Small flushing rate would mean a longer retention time of pollutant and phytoplankton inside the bay, which provides a favourable environment for algal blooms. Moreover, vertical mixing can also significantly affect the suspension and migration of phytoplankton and their efficiency in utilising nutrient and solar radiation. Our field observations have shown that vertical structures of phytoplankton are important features of algal blooms.

In eutrophic and weakly-flushed sub-tropical coastal waters in Hong Kong, the optimal algal growth rate is often much greater than the mortality and flushing losses. Under favourable environmental conditions, a bloom can always occur based on purely biological considerations. The tendency to bloom, however, is negated by effects of vertical mixing and settling. We have put forward a model to derive practical metrics for the assessment of the likelihood of algal blooms in Hong Kong waters. The model encapsulates the essential biological processes of algal growth and settling, and light and nutrient utilisation, and hydrodynamic vertical mixing into a simple mathematical framework. The model requires only readily available field measurements of water column transparency, nutrient concentration, representative maximum algal growth rate, and simple estimate of vertical mixing as a function of tidal range, wind speed, and density stratification. The model predictions are validated by field observations of this and previous studies. By applying the model to long-term monitoring data, it is also possible to explain the occurrence of the two types of blooms in relation to the vertical turbulence and background pollution characteristics at the algal bloom black spots. The algal bloom forecast criterion (Eq. 15) has also been validated against a 20-year long-term water quality data set for Hong Kong waters (Wong and Lee, 2006b). The model proved invaluable in explaining the complex myriad of spatial and temporal patterns of observed algal bloom occurrences in the coastal waters around Hong Kong.

This work is a first step towards developing a real-time HAB forecasting system. In the Hong Kong context, such a system may be designed as follows:

(1) In a mariculture zone, we can make daily measurements of Secchi disk depth and water temperature. The stability criterion for diatoms can then be easily checked using the Secchi disk depth and representative growth rates (adjusted for water temperature). The turbulent diffusivity of a particular tidal inlet can also be determined expediently as a function of tidal range and wind (an elaborate calculation has to be done once for a given site). It is then possible to check every day whether the estimated diffusivity is lower than the stability threshold. This simple step alone will give a lot of information on algal bloom risks.
(2) An automatic nutrient analyzer can be incorporated into the telemetry system to determine the nutrient level, and the risk of a diatom bloom can be assessed via the stability criterion.
(3) Given a representative dinoflagellate growth rate (adjusted for temperature) and assumed algal nutrient concentration C_N, the likelihood of a dinoflagellate bloom can be assessed (via the nutrient competition threshold).
(4) Once a bloom risk is identified, the fish farmers can be alerted to look out for possible signs or conditions favourable for algal blooms (e.g. unusual calm sea, visible pollution).
(5) Finally, if an extensive bloom is observed, hydrodynamic tracking can also be initiated to forecast the likely path and affected areas in the next day or so (see Lee and Qu, 2004).

Thus the simple model outlined herein can serve as the engine of a more elaborate early warning system; past experience with major environmental disasters in the Pearl River Delta suggests that early alerts with even one day of lead time can be highly beneficial for environmental management and control.

Acknowledgements

This work is supported by a Hong Kong Research Grants Council (RGC) Central Allocation Group Research Project (HKU 2/98C and 1/02C), and partially by a grant from the University Grants Committee of the Hong Kong Special Administrative Region, China (Project No. AoE/P-04/04). The support of the Agriculture, Fisheries and Conservation Department

(AFCD) and the Environmental Protection Department (EPD) of the Hong Kong Government are gratefully acknowledged. The many stimulating discussions with Dr. Patsy Wong and research staff of AFCD are well-appreciated.

References

Anderson, D.M., 1994. Red tides. Scientific American 271, 62–68.

Bowden, K.F., 1983. Physical Oceanography of Coastal Waters. Horwood, Chichester, 302 pp.

Bowie, G.L., Mills, W.B., Porcella, D.B., Campbell, C.L., Pagenkopf, J.R., Rupp, G.L., Johnson, K.M., Chan, P.W.H., Gherini, S.A., 1985. Rates Constants and Kinetics Formulations in Surface Water Quality Modeling (second ed.). Rep. EPA 600/3–85/40, U.S. EPA, Athens, Georgia, 455 pp.

Choi, D.K.W., Lee, J.H.W., 2004. Numerical determination of flushing time for stratified waterbodies. Journal of Marine Systems 50, 263–281.

Cullen, J.J., Horrigan, S.G., 1981. Effects of nitrate on the diurnal vertical migration, carbon to nitrogen ratio, and the photosynthetic capacity of the dinoflagellate *Gymnodinium splendens*. Marine Biology 62, 81–89.

Cullen, J.J., MacIntyre, J.G., 1998. Behaviour, physiology and the niche of depth-regulating. In: Anderson, D.M., Cembella, A.D., Hallegraeff, G.M. (Eds.), Physiological Ecology of Harmful Algal Blooms. Springer, Berlin, pp. 559–579.

Di Toro, D.M., 1974. Vertical interactions in phytoplankton populations—an asymptotic Eigenvalue analysis (IFYGL). Proceedings of the 17th Conference on Great Lakes Research. International Association for Great Lakes Research, pp. 17–27.

Droop, M.R., 1973. Some thoughts on nutrient limitation in algae. Journal of Phycology 9, 254–272.

Estrada, M., Alcaraz, M., Marrase, C., 1987. Effects of turbulence on the composition of phytoplankton assemblages in marine microcosms. Marine Ecology Progress Series 38, 267–281.

Fischer, H.B., List, E.J., Koh, R.C.Y., Imberger, J., Brooks, N.H., 1979. Mixing in Inland and Coastal Waters. Academic Press, New York, 483 pp.

Hallegraeff, G.M., 1993. A review of harmful algal blooms and their apparent global increase. Phycologia 32, 79–99.

Hamrick, J.M., 1992. A three-dimensional Environmental Fluid Dynamics Computer Code: theoretical and computational aspects. Special Report 317, The College of William and Mary, Virginia Institute of Marine Science.

Hodgkiss, I.J., Ho, K.C., 1997. Are changes in N:P ratios in coastal waters the key to increased red tide blooms. Hydrobiologia 352, 141–147.

Huisman, J., van Oostveen, P., Weissing, F.J., 1999. Critical depth and critical turbulence: two different mechanisms for the development of phytoplankton blooms. Limnology and Oceanography 44, 1781–1787.

James, I.D., 1977. A model of the annual cycle of temperature in a frontal region of the Celtic Sea. Estuarine and Coastal Marine Science 5, 339–353.

Jorgensen, S.E., 1979. Handbook of Environmental Data and Ecological Parameters, first ed. Pergamon Press, Oxford, 1162 pp.

Lee, H.S., Lee, J.H.W., 1995. Continuous monitoring of short-term dissolved oxygen and algal dynamics. Water Research 29, 2789–2796.

Lee, J.H.W., Qu, B., 2004. Hydrodynamic tracking of the massive spring 1998 red tide in Hong Kong. Journal of Environmental Engineering. ASCE 130, 535–550.

Lee, J.H.W., Hodgkiss, I.J., Wong, K.T.M., Lam, I.H.Y., 2005. Real time observations of coastal algal blooms by an early warning system. Estuarine, Coastal and Shelf Science 65, 172–190.

Lee, J.H.W., Harrison, P.J., Kuang, C.P., Yin, K.D., 2006. Eutrophication dynamics in Hong Kong waters: physical-biological interactions. In: Wolanski, E. (Ed.), The Environment in Asia Pacific Harbours. Springer, Berlin, pp. 187–206.

Levandowsky, M., Kaneta, P.J., 1987. Behaviour in dinoflagellates. In: Taylor, F.J.R. (Ed.), The Biology of Dinoflagellates, Botanical Monographs, vol. 21. Blackwell Scientific Publications, London, pp. 360–397.

Lewis, R., 1997. Dispersion in Estuaries and Coastal Waters. Wiley, Chichester, 312 pp.

Margalef, R., 1978. Life form of phytoplankton as survival alternatives in an unstable environment. Oceanologica Acta 1, 493–509.

Margalef, R., Estrada, M., Blasco, D., 1979. Functional morphology of organisms involved in red tides, as adapted to decaying turbulence. In: Taylor, D.L., Seliger, H.H. (Eds.), Toxic Dinoflagellate Blooms, Proceedings of the Second International Conference on Toxic Dinoflagellate Blooms. Elsevier, North Holland, pp. 89–94.

Munk, W.H., Anderson, E.R., 1948. Notes on the theory of the thermocline. Journal of Marine Research 1, 7276–7295.

Paerl, H.W., 1988. Nuisance phytoplankton blooms in coastal, estuarine, and inland waters. Limnology and Oceanography 33, 823–847.

Peters, F., Marrase, C., 2000. Effects of turbulence on plankton: an overview of experimental evidence and some theoretical considerations. Marine Ecology Progress Series 205, 291–306.

Pinegree, R.D., Holligan, P.M., Mardell, G.T., Head, R.N., 1976. The influence of physical stability on spring, summer and autumn phytoplankton blooms in the Celtic Sea. Journal of the Marine Biology Association, UK 56, 845–873.

Reynolds, C.S., 1987. Community organization in the freshwater plankton. British Ecological Society Symposium 27, 297–325.

Roache, P.J., 1998. Fundamentals of Computational Fluid Dynamics. Hermosa Publishers, Albuquerque, NM, 648 pp.

Riley, G.A., Stommel, H., Bumpus, D.F., 1949. Quantitative ecology of the plankton of the western North Atlantic. Bulletin of the Bingham Oceanographic Collection Yale University 12, 1–169.

Ryther, J.H., 1955. Ecology of autotrophic marine dinoflagellates with reference to red water conditions. In: Johnson, F.H. (Ed.), The Luminescence of Biological Systems. American Association of the Advancement for Science, New York, pp. 387–413.

Schnoor, J.L., Di Toro, D.M., 1980. Differential phytoplankton sinking- and growth-rates: an Eigenvalue analysis. Ecological Modelling 9, 233–245.

Smayda, T.J., 1970. The suspension and sinking of phytoplankton in the sea. Oceanography and Marine Biology 8, 353–414.

Smayda, T.J., 1997a. Harmful algal blooms: their ecophysiology and general relevance to phytoplankton blooms in the sea. Limnology and Oceanography 42, 1137–1153.

Smayda, T.J., 1997b. What is a bloom? A commentary. Limnology and Oceanography 42, 1132–1136.

Smayda, T.J., 2002. Adaptive ecology, growth strategies and the global bloom expansion of dinoflagellates. Journal of Oceanography 58, 281–294.

Sverdrup, H.U., 1953. On conditions for the vernal blooming of phytoplankton. ICSE Journal of Marine Science 18, 287–295.

Thomas, W.H., Gibson, C.H., 1990. Effects of small-scale turbulence on microalgae. Journal of Applied Phycology 2, 71–77.

Thomann, R.V., Mueller, J.A., 1987. Principles of Surface Water Quality Modeling and Control. Harper & Row, New York, 644 pp.

Watanabe, M., Kohata, K., Kimura, T., Takamatsu, T., Yamaguchi, S., Ioriya, T., 1995. Generation of a *Chattonella antiqua* bloom by imposing a shallow nutricline in a mesocosm. Limnology and Oceanography 40, 1447–1460.

White, A.W., 1976. Growth inhibition caused by turbulence in the toxic marine dinoflagellate *Gonyaulax excavata*. Journal of the Fisheries Research Board of Canada 33, 2598–2602.

Wong, K.T.M., 2004. Red tides and algal blooms in subtropical Hong Kong waters: field observations and Lagrangian modeling, Ph.D. thesis, The University of Hong Kong, Hong Kong.

Wong, K.T.M., Lee, J.H.W., 2003. A novel Lagrangian particle method for advective diffusion transport problem. 16th ASCE Engineering Mechanics Conference, July 16–18, 2003, University of Washington, Seattle (CD-ROM).

Wong, K.T.M., Lee, J.H.W., 2006a. Cell quota based algal dynamics model using a deterministic Lagrangian particle method. Seventh

International Conference on Hydroinformatics, Nice, September 3–8, 2006, pp. 534–541.

Wong, K.T.M., Lee, J.H.W., 2006b. Forecasting of environmental risk maps of harmful algal blooms in semi-enclosed coastal waters. Proceedings of the Second International Conference on Estuaries and Coasts, Guangzhou, China, November 28–30, 2006, vol. 1, pp. 103–111.

Yang, Z.B., Hodgkiss, I.J., 2004. Hong Kong's worst red tide—causative factors reflected in a phytoplankton study at Port Shelter station in 1998. Harmful Algae 3, 149–161.

Yin, K., 2003. Influence of monsoons and oceanographic processes on red tides in Hong Kong waters. Marine Ecology Progress Series 262, 27–41.